Electronic Supplementary Material (ESI) for Dalton Transactions.

Magnetic Anisotropy in Octahedral Dy(III) and Yb(III) complexes

Aditya Borah, Sourav Dey, Kehkasha Siddiqui, Sandeep K. Gupta, Gopalan Rajaraman* and Ramaswamy Murugavel*

Experimental Section

Instruments and Methods

All the reactions were performed at ambient reaction conditions. Fourier-transform infrared spectra were recorded on a Perkin Elmer Spectrum One spectrometer using KBr diluted pellets. The ESI-MS studies were carried out on Bruker MaXis impact mass spectrometer. Microanalyses were performed on a Thermo Finnigan (FLASH EA 1112) microanalyzer. Powder X-ray diffractions were recorded on a Philips X'pert Pro (PANalytical) diffractometer using Cu Kα radiation (λ = 1.54190 Å). The simulated PXRD patterns have been generated from the .res file of the respective crystal data using Mercury 2022.1.0 software. NMR spectra were recorded using a Bruker Advance DPX-400 spectrometer. The magnetic properties of the polycrystalline samples (~30 mg of the samples are packed in Teflon) were measured using a Quantum Design MPMS-XL SQUID magnetometer equipped with a 7 T magnet in the temperature range of 2-300 K. The data were corrected for the background diamagnetic contribution and the diamagnetic contribution of the compounds was corrected using Pascal's constants. Alternating current (ac) susceptibility measurements were performed with an oscillating ac field of 3.5 Oe oscillating at indicated frequencies between 0.1 and 1500 Hz. The dc and ac susceptibility measurements of 20% diluted sample of **1** have been carried out on Quantum Design PPMS Dynacool equipped with a 9T magnet within the frequency range of 100-4500 Hz.

Materials

Commercial grade solvents were purified by employing conventional procedures[1]. Lanthanide nitrates, 2, 6-diisopropylphenol, and phosphorous oxychloride were procured from commercial sources and used as received. 2,6-Diisopropylphenyl phosphate was synthesized as described previously in the literature.[2]

Single crystal X-ray crystallography

Suitable single crystals of **1** and **2** were selected and mounted on a Rigaku Saturn 724+ CCD diffractometer for unit cell determination and intensity data collection. Data integration and indexing were carried out using CrysAlisPro software. Using Olex[3], the structure was solved with the ShelXT[4] structure solution program using Intrinsic Phasing. The complete refinement of the structures was carried out with the ShelXL[5] refinement package using Least Squares minimization. All non-hydrogen atoms were refined anisotropically. The hydrogen atoms were refined isotropically as rigid atoms in their idealized locations.

***General procedure for the synthesis of compounds* 1-3**

To the solution of $Ln(NO_3)_3.xH_2O$ (0.25mmol) in water (5 mL) and methanol (10 mL), $dippH_2$ (258 mg, 1 mmol) in methanol (10 mL) solution was added. The solution was stirred at room temperature till the solution became slightly hazy due to the formation of a precipitate (usually 3-4 hrs). The solution was allowed to stand undisturbed overnight to settle down all the fine precipitate. The solution was filtered carefully and the clear solution is kept for crystallization in aerobic conditions at room temperature. Very slow evaporation of the solvent leads to the formation of rectangular-prism-shaped crystals in 3-4 weeks. During the crystallization process, the solution was repeatedly filtered until there is no precipitate occurs.

***Characterization of* 1**. yield: 30 mg (13% based on ligand) m.p. > 250 ^oC; *m/z* = 1710.53 $(M+H)^+$; FTIR (KBr, cm^{-1}) : 3597 (s), 3551 (br), 3067 (w), 2968 (s), 2870 (m), 2343 (br), 1622 (br), 1466 (s), 1444 (s), 1363 (s), 1334 (s), 1257 (s), 1175 (vs), 1084 (s), 962 (vs), 799 (s), 772 (vs), 662 (s), 538 (s), 504 (vs); Anal. Calculated (Found): $C_{72}H_{111}O_{24}P_6Dy_1.3(H_3O_2)$: C, 47.59 (47.72) H, 6.82 (6.62)

***Characterization of* 2.** yield: 41 mg (18% based on ligand) m.p. > 250 ^oC; m/z = 1720.51 $(M+H)^+$; FTIR (KBr, cm^{-1}) : 3604 (s), 3535 (br), 3070 (w), 2969 (s), 2874 (s), 2322 (br), 1632 (br), 1470 (s), 1440 (s), 1385 (s), 1339 (s), 1257 (s), 1190 (vs), 1098 (s), 954 (s), 801 (s), 766 (vs), 658 (s), 535 (vs), 502 (vs); Anal. Found (Calculated) : $C_{72}H_{111}O_{24}P_6Yb_1$. $6H_2O$: C, 47.34 (47.32) H, 6.41 (6.78).

***Characterization of* 3.** Yield: ~30 mg (16% based on ligand). m.p. > 250 ^oC ; *m/z* = 1635.45 $(M+H)^+$; FTIR (KBr, cm^{-1}): 3602 (s), 3531 (br), 3066 (w), 2970 (s), 2871 (m), 2298 (br), 1644 (br), 1466 (s), 1440 (s), 1339 (s), 1254

(s), 1189 (vs), 1113 (s), 1097 (s), 954 (vs), 801 (s), 765 (vs), 658 (s), 535 (s), 501 (vs); Anal. Found (Calculated) for $C_{72}H_{111}O_{24}P_6Y_1.3H_2O$: C, 50.99 (51.19), 7.06 (6.98). ^{31}P NMR (CD_3OD): δ – 7.28 ppm

***Synthesis of compounds* 1Y**

To the solution of $Dy(NO_3)_3.xH_2O$ (0.05 mmol) and $Y(NO_3)_3.xH_2O$ (0.15 mmol) in water (5 mL) and methanol (10 mL), $dippH_2$ (258 mg, 1 mmol) in methanol (10 mL) solution was added. The solution was stirred at room temperature till the solution became slightly hazy due to the formation of a precipitate (usually 3-4 hrs). The solution was allowed to stand undisturbed overnight to settle down all the fine precipitate. The solution was filtered carefully and the clear solution is kept for crystallization in aerobic conditions at room temperature. Very slow evaporation of the solvent leads to the formation of rectangular-prism-shaped crystals in 3-4 weeks. During the crystallization process, the solution was repeatedly filtered until there is no precipitate occurs. ICP-AES analysis has been carried out to find the extent of dilution, confirming that **1Y** contains approximately 20% of **1** in the matrix of **3**.

***Characterization of* 1Y.** Yield: ~25 mg (18% based on ligand). m.p. > 250 ^oC; FTIR (KBr, cm^{-1}): 3600 (s), 3532 (br), 3065 (w), 2970 (s), 2871 (s), 2300 (br) 1635 (br), 1465 (s), 1441 (s), 1384 (vs), 1338 (s), 1257 (s), 1171 (vs), 1095 (s), 1046 (s), 955 (s), 799 (s), 765 (vs), 658 (s), 533 (s), 501 (vs).

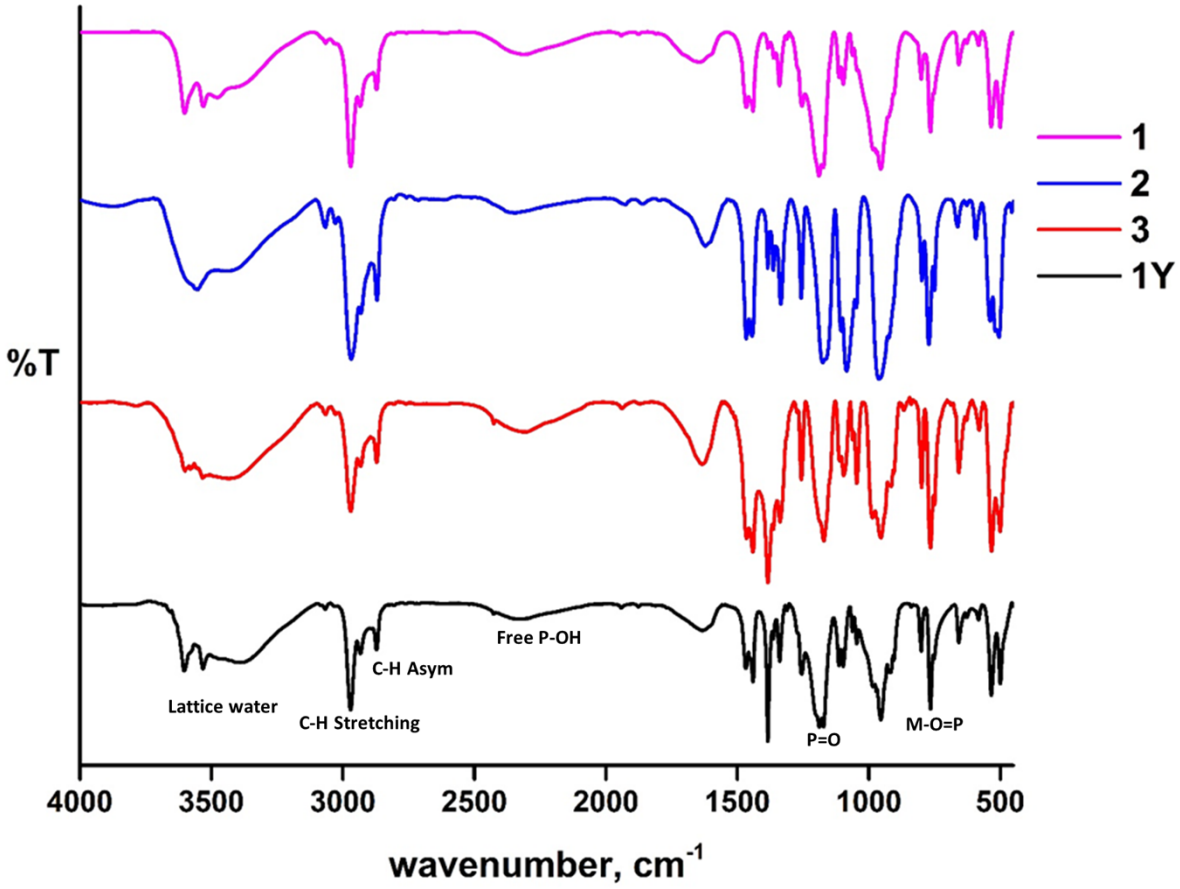

Figure - S1. FTIR spectra of the complexes **1-3, 1Y** as disc diluted with KBr.

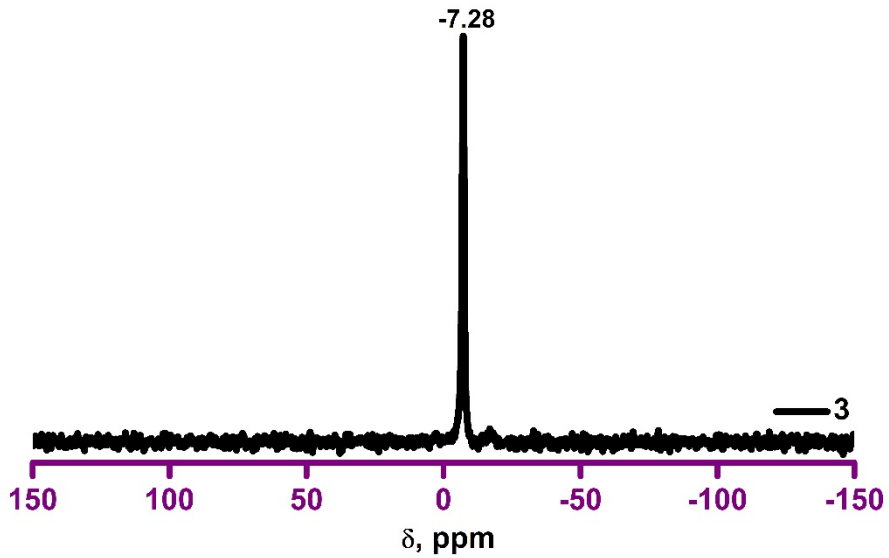

Figure - S2. ^{31}P NMR of **3** in CD_3OD

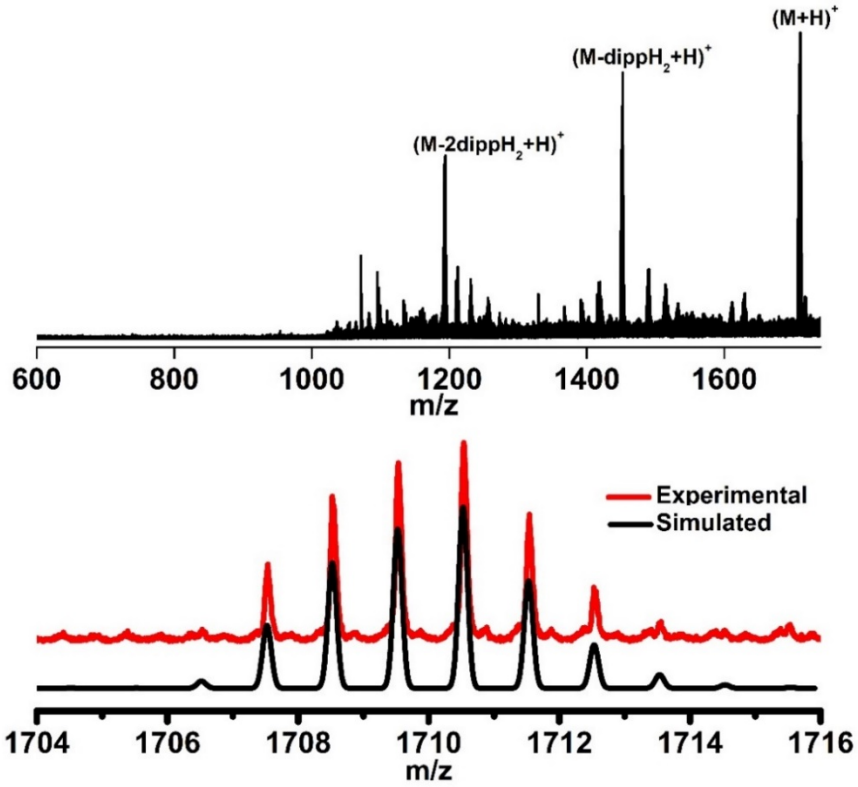

Figure – S3. ESI - MS spectrum of **1** in methanol. The full spectrum is shown on top and the molecular ion peak is shown at bottom.

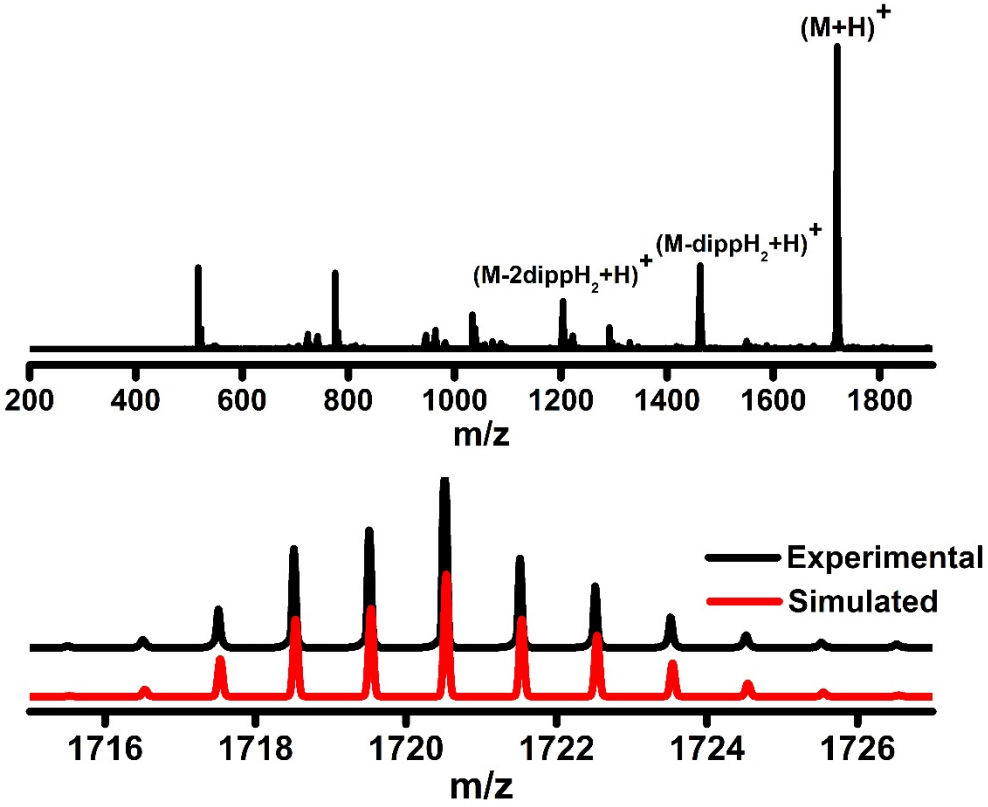

Figure – S4. ESI - MS spectrum of **2** in methanol. The full spectrum is shown on top and the molecular ion peak is shown at bottom.

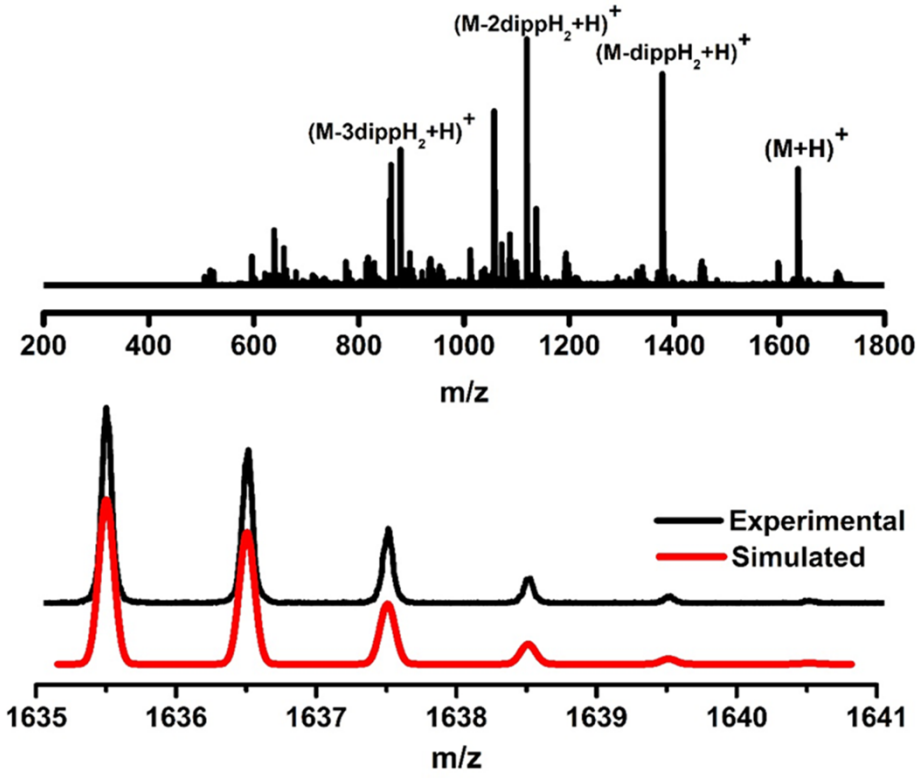

Figure – S5. ESI - MS spectrum of **3** in methanol. The full spectrum is shown on top and the molecular ion peak is shown at bottom.

Table S1. Crystal Data and Structure Refinement Details for **1-3**

Identification code	**1**	**2**	**3**
CCDC No.	2069003	2069009	2331545
Empirical formula	$C_{72}H_{123}DyO_{30}P_6$	$C_{72}H_{123}O_{30}P_6Yb$	$C_{72}H_{123}O_{30}P_6Y$
Formula weight	1817.02	1827.56	1743.43
Temperature/K	150.0	150.0	150
Crystal system	trigonal	trigonal	trigonal
Space group	$R\bar{3}$	$R\bar{3}$	$R\bar{3}$
a/Å	23.764(4)	23.5532(3)	23.5867(4)
b/Å	23.764(4)	23.5532(3)	23.5867(4)
c/Å	13.421(4)	13.4632(2)	13.2999(2)
α/°	90	90	90
β/°	90	90	90
γ/°	120	120	120
Volume/Å^3	6564(3)	6468.1(2)	6407.9(2)
Z	3	3	3
ρ_{calc}g/cm^3	1.379	1.408	1.355
μ/mm^{-1}	1.039	1.273	0.873
F(000)	2853.0	2865.0	2772.0
Crystal size/mm^3	0.18 × 0.19 × 0.35	0.20 × 0.20 × 0.40	0.22×0.25× 0.45
Radiation	MoK*α* (λ = 0.71073)	MoK*α* (λ = 0.71073)	MoKα(λ = 0.71073)
2Θ range for data collection/°	4.988 to 49.976	5.01 to 49.98	5.028 to 49.998
Index ranges	-28 ≤ h ≤ 27, -20 ≤ k ≤ 28, -15 ≤ l ≤ 15	-28 ≤ h ≤ 21, -28 ≤ k ≤ 28, -15 ≤ l ≤ 15	-28 ≤ h ≤ 28, -28 ≤ k ≤ 22, -15 ≤ l ≤ 15
Reflections collected	11886	14642	22371
Independent reflections	2568 [R_{int} = 0.0274, R_{sigma} = 0.0173]	2523 [R_{int} = 0.0507, R_{sigma} = 0.0361]	2502 [R_{int} = 0.0422, R_{sigma} = 0.0216]
Data/restraints/parameters	2568/0/178	2523/0/175	2502/3/176
Goodness-of-fit on F^2	1.063	1.079	1.072
Final R indexes [I>=2σ (I)]	R_1 = 0.0186, *w*R_2 = 0.0498	R_1 = 0.0306, *w*R_2 = 0.0679	R_1 = 0.0331, wR_2 = 0.0911
Final R indexes [all data]	R_1 = 0.0186, *w*R_2 = 0.0499	R_1 = 0.0313, *w*R_2 = 0.0685	R_1 = 0.0343, *w*R_2 = 0.0922
Largest diff. peak/hole / e Å^{-3}	0.26/-0.31	0.39/-0.52	0.56/-0.57

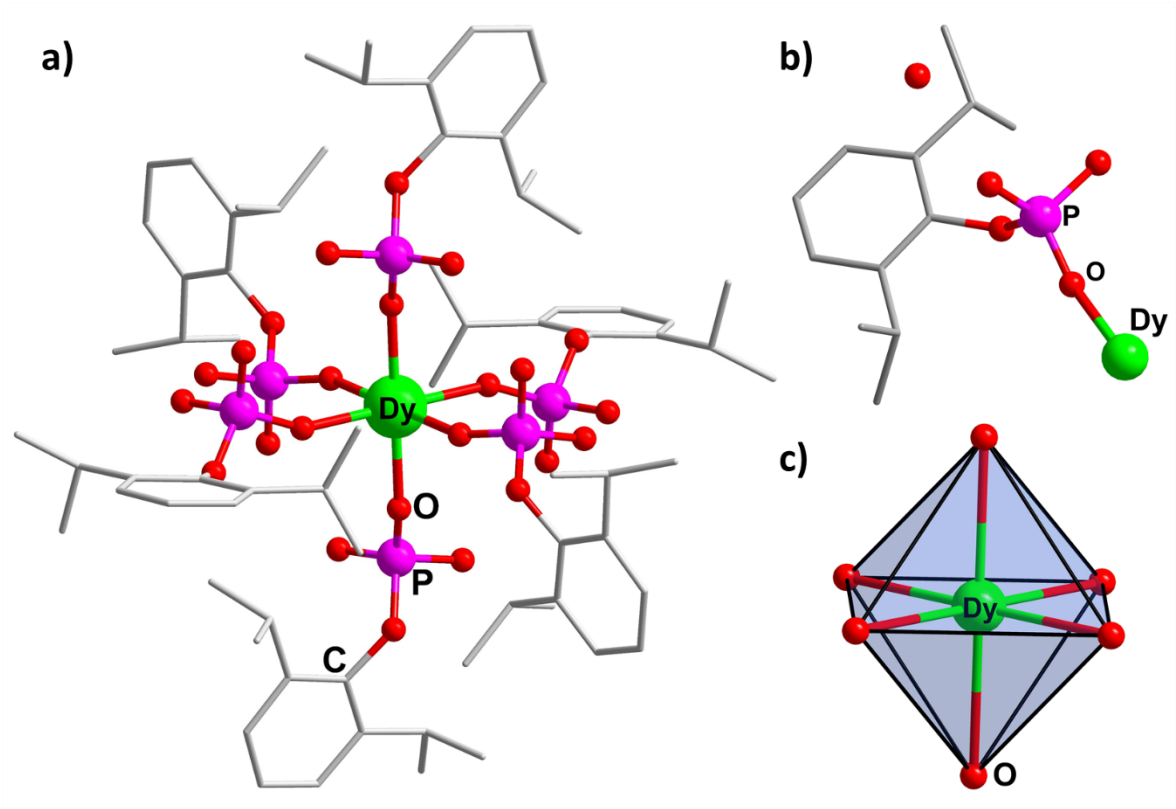

Figure S6. a) Molecular structure of **1**. Lattice $(H_5O_2)^+$ molecules and hydrogen atoms are omitted for clarity. (b) Asymmetric unit of **1**. It contains one Dy(III) centre with one of the six phosphate ligands and half of $(H_5O_2)^+$ molecule. The hydrogen atoms are omitted for clarity. (c) The coordination environment of Dy(III) ion in **1.**

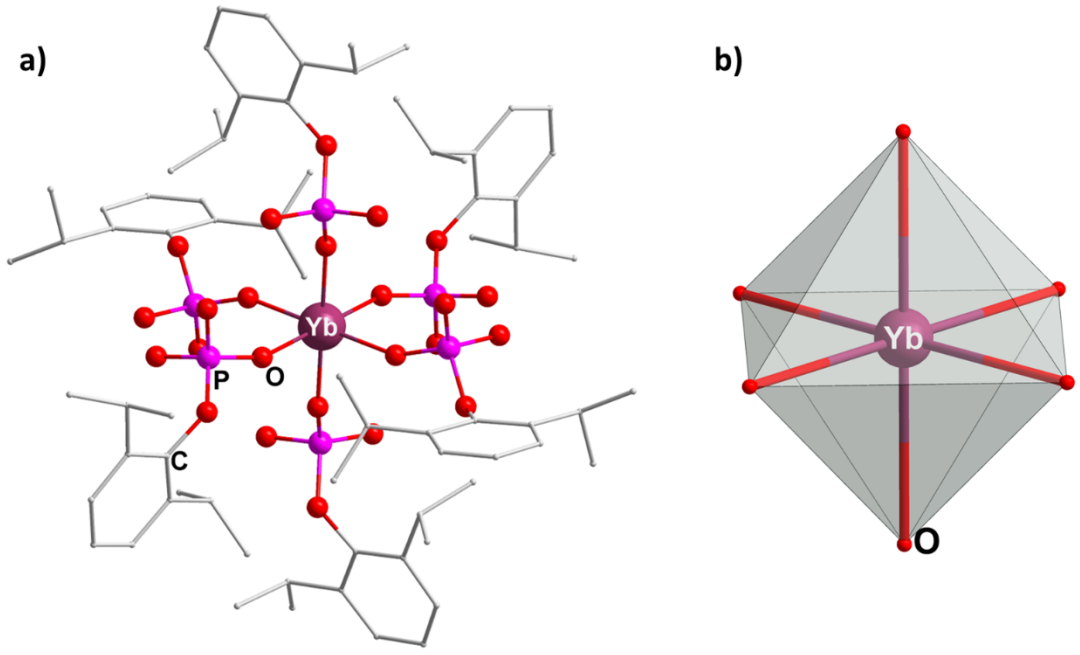

Figure S7. a) molecular structure of **2**. Lattice $(H_3O_2)^-$ moieties and hydrogen atoms are omitted for clarity. (b) The octahedral shaped coordination environment of Yb(III) ion in **2.**

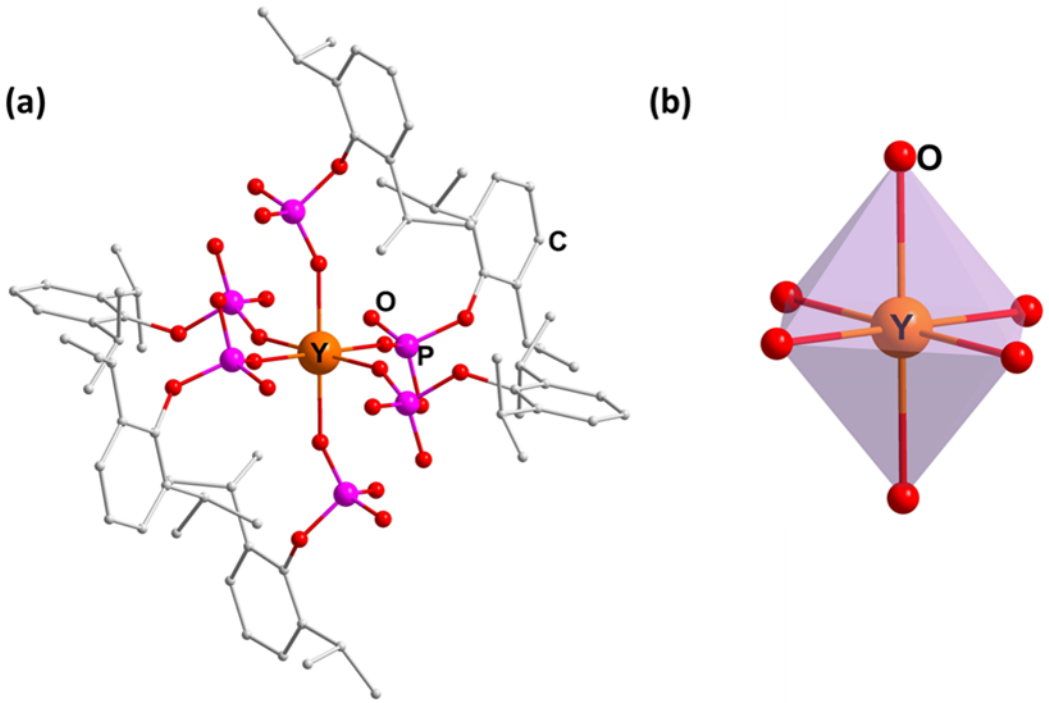

Figure S8. a) molecular structure of **3**. Lattice $(H_5O_2)^+$ moieties and hydrogen atoms are omitted for clarity. (b) The octahedral shaped coordination environment of Y(III) ion in **3.**

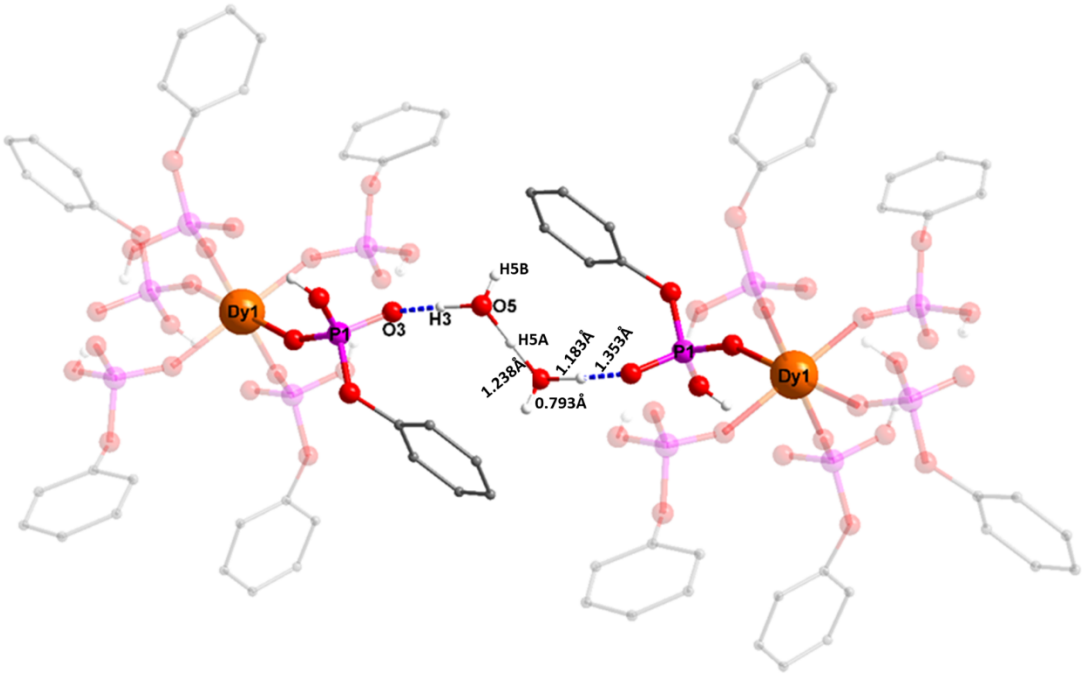

Figure S9A: The lattice water molecule is close to the phosphate oxygen (O3). H3 atom can move to-and-fro between O3(P3) and O5(water). In case of **1**, H3 is closer to O5, as compared to O3 producing $(H_5O_2)^+$ cations. Only one of the six $(H_5O_2)^+$ cations is shown for clarity. The isopropyl group on phenyl ring, H atoms attached to carbon atoms are omitted for clarity. The bond lengths related to the $(H_5O_2)^+$ species is indicated in the figure.

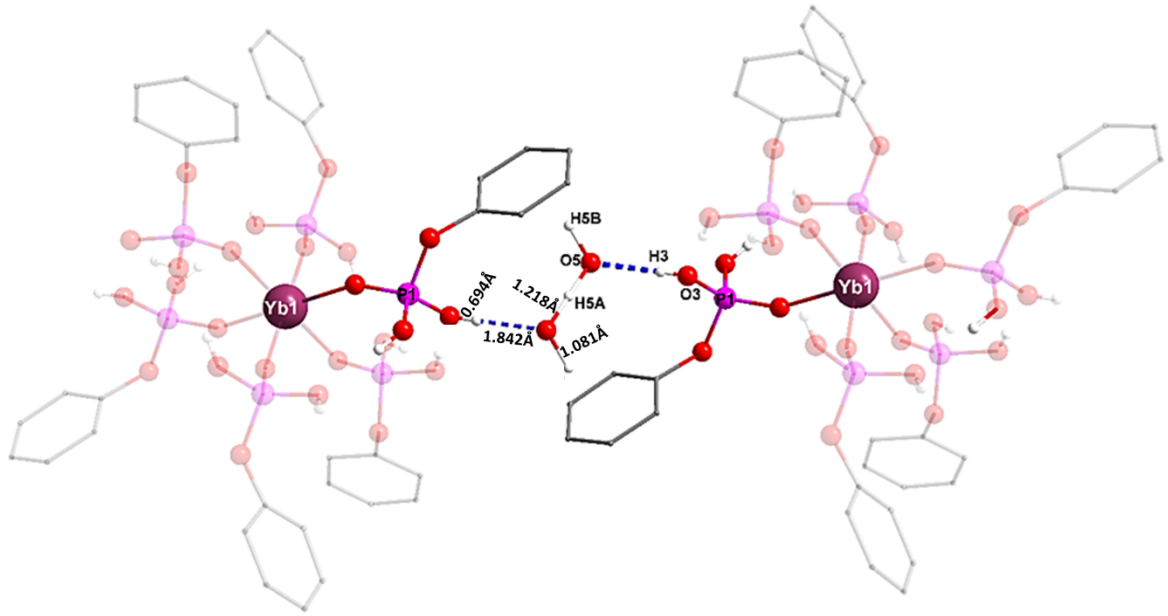

Figure S9B: H3 is closer to O3(P1), as compared to O5 in case of **2**, producing $(H_3O_2)^-$ anions. Only one of the six $(H_3O_2)^-$ anions is shown for clarity. The isopropyl group on phenyl ring, H atoms attached to carbon atoms are omitted for clarity. The bond lengths related to the $(H_3O_2)^-$ species is indicated in the figure.

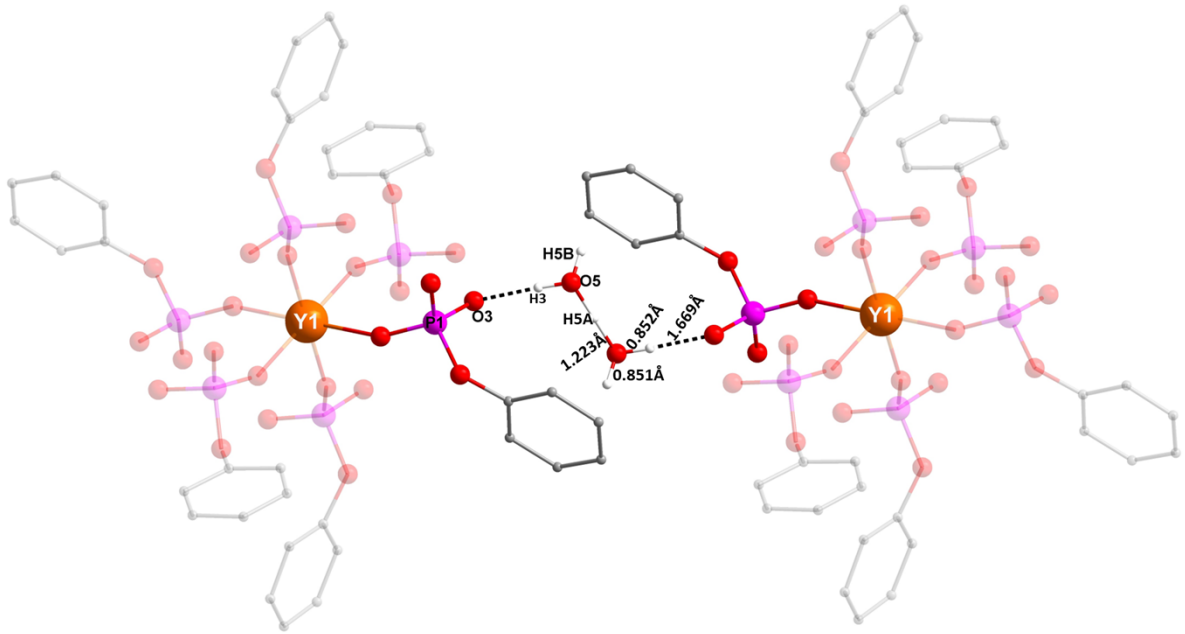

Figure S9C: H5A is closer to O5, as compared to O3(P1) in case of **3**, producing $(H_5O_2)^+$ cation. Only one of the six $(H_5O_2)^+$ cations is shown for clarity, along with the bond lengths. The isopropyl group on phenyl ring, H atoms attached to carbon atoms are omitted for clarity.

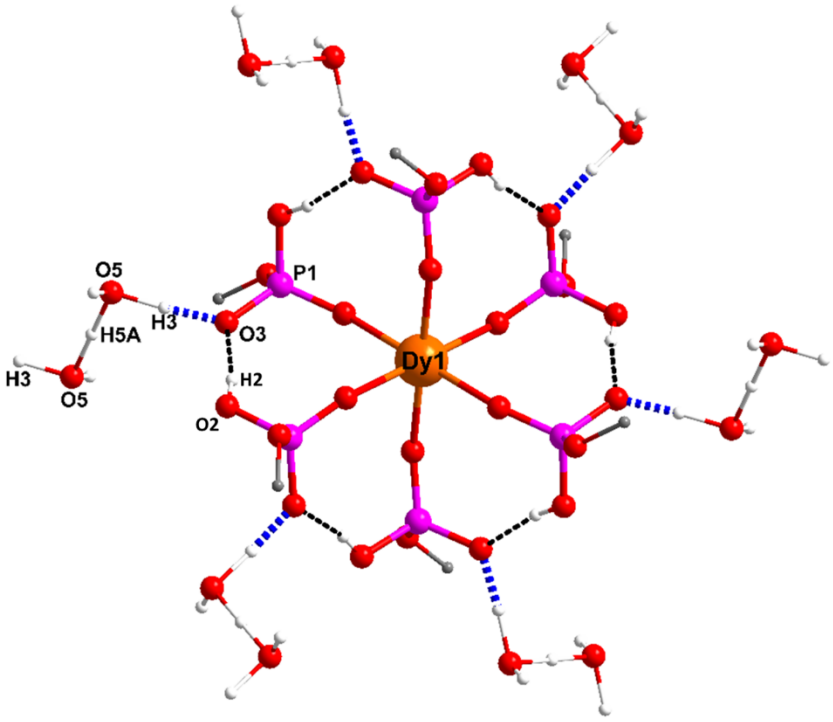

Figure S10: Extensive intramolecular (black dotted bonds) and intermolecular (blue dotted bonds) H-bonding in **1**. The carbon atoms of the phenyl ring (except the carbon atom attached to the phosphate group) as well as the isopropyl groups are omitted for clarity. The H atoms which are not involved in intermolecular and intermolecular H bonding are also omitted.

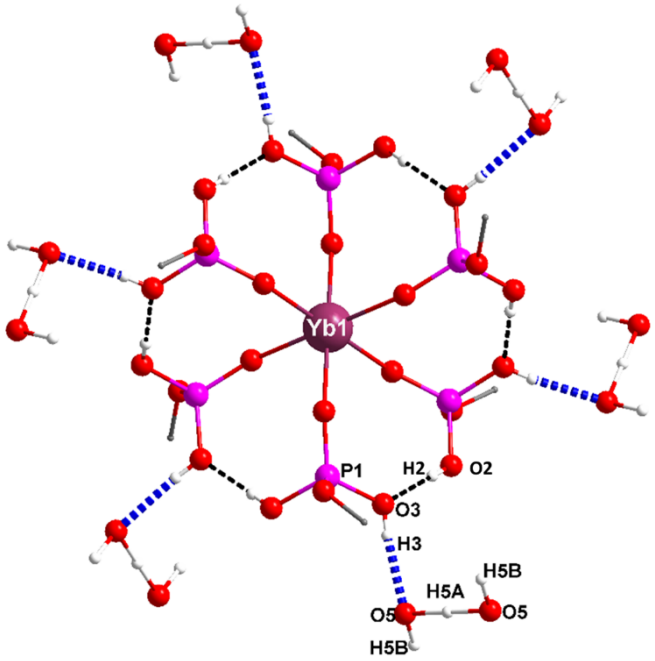

Figure S11: Extensive intramolecular (black dotted bonds) and intermolecular (blue dotted bonds) H-bonding in **2**. The carbon atoms of the phenyl ring (except the carbon atom attached to the phosphate group) as well as the isopropyl groups are omitted for clarity. The H atoms which are not involved in intermolecular and intermolecular H bonding are also omitted.

Table S2: Hydrogen bonding interactions in **1-3** (in Å and °)

	1	**2**	**3**
O5-H5A	1.238	1.218	1.223
O5-H5B	0.79	1.081	0.851
O5-H3	1.183	1.842	0.852
O3-H3	1.353	0.694	1.669
O5-O5’	2.476	2.436	2.446
O5-H3-O3	174.38	172.76	175.03
O5-H5A-O5’	180	180	180

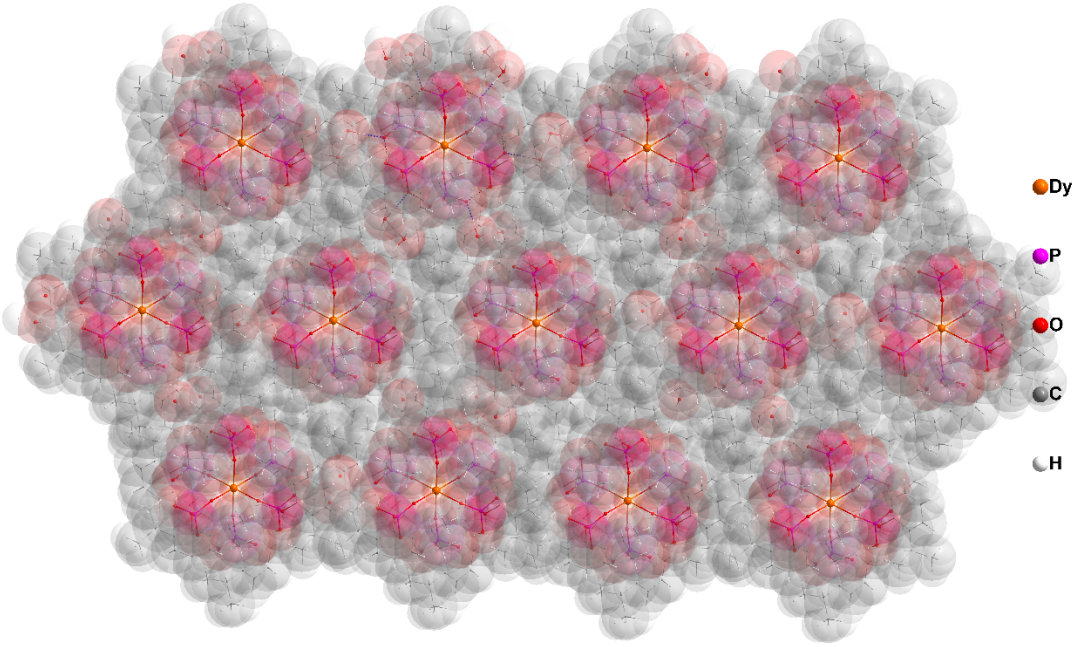

Figure S12A. Space-fill model showing the lattice arrangement of **1**. Each of the six coordinated molecule of **1** is surrounded by six lattice $(H_5O_2)^+$ moieties followed by six molecules of **1.**

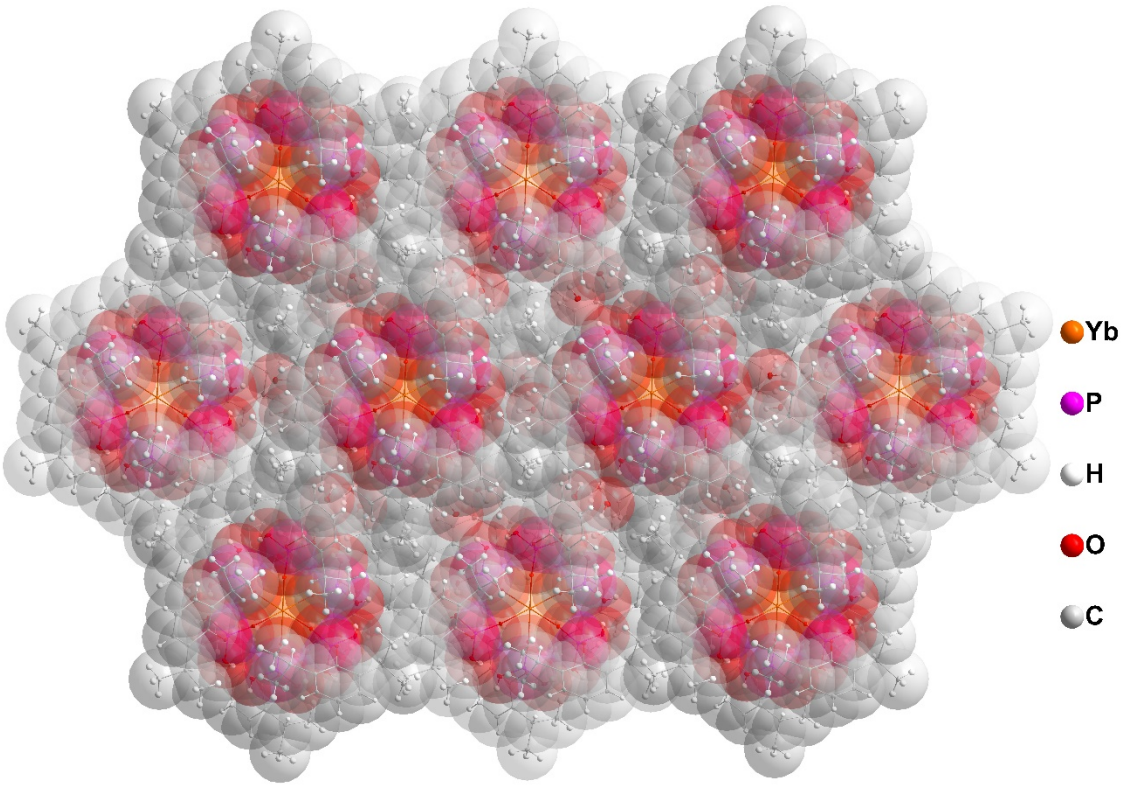

Figure S12B. Space-fill model showing the lattice arrangement of **2**. Each of the six coordinated molecule of **2** is surrounded by six lattice $(H_3O_2)^-$ moieties followed by six molecules of **2.**

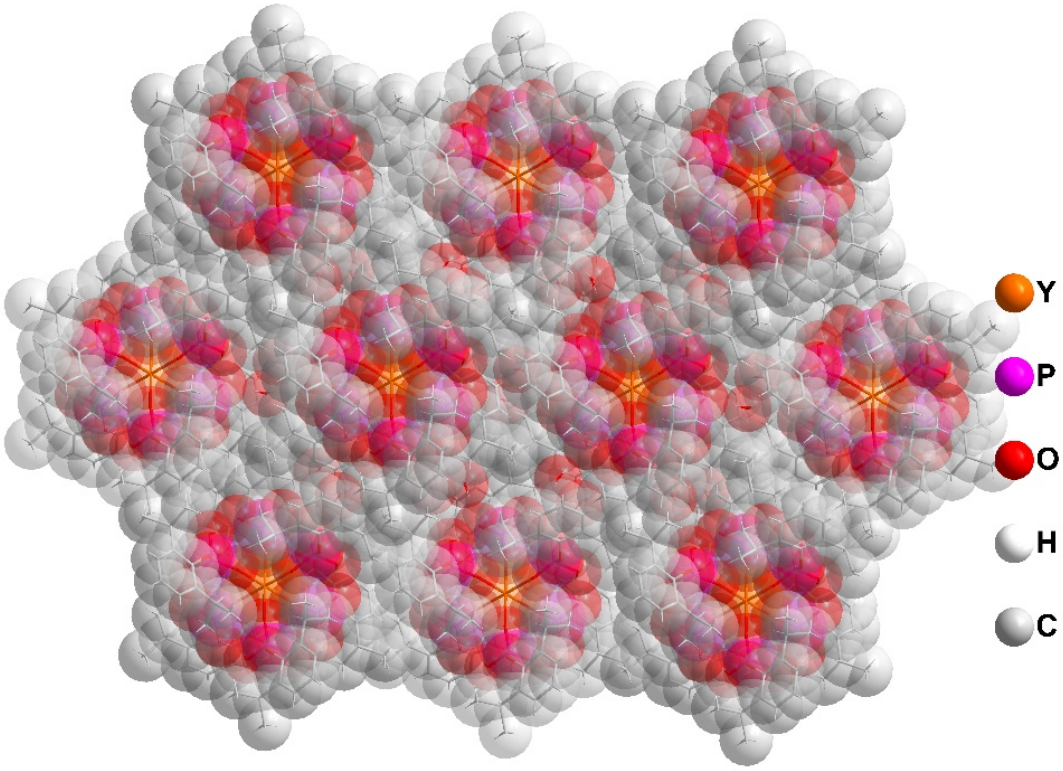

Figure S12C. Space-fill model showing the lattice arrangement of **3**. Each of the six coordinated molecule of **3** is surrounded by six lattice $(H_5O_2)^+$ moieties followed by six molecules of **3.**

Table S3: Selected bond lengths (Å) and bond angles (°) in **1**

Dy1-O1^{1}	2.2428(2)	P1-O4	1.5842(3)	O1^{2}-Dy1-O1	92.55(5)
Dy1-O1^{2}	2.2428(2)	O1^{1}-Dy1-O1^{2}	92.55(5)	O1^{3}-Dy1-O1	87.45(5)
Dy1-O1^{3}	2.2428(2)	O1^{1}-Dy1-O1	92.55(5)	O1^{2}-Dy1-O1^{5}	87.45(5)
Dy1-O1	2.2428(2)	O1^{1}-Dy1-O1^{3}	180.0	O1^{5}-Dy1-O1^{3}	92.55(5)
Dy1-O1^{4}	2.2428(2)	O1^{4}-Dy1-O1^{3}	92.55(5)	O1^{2}-Dy1-O1^{3}	87.45(5)
Dy1-O1^{5}	2.2428(2)	O1^{5}-Dy1-O1^{4}	92.55(5)	O1^{2}-Dy1-O1^{4}	180.0
P1-O1	1.4889(3)	O1^{4}-Dy1-O1	87.45(5)	O1^{1}-Dy1-O1^{4}	87.45(5)
P1-O2	1.5524(5)	O1^{1}-Dy1-O1^{5}	87.45(5)		
P1-O3	1.5056(5)	O1^{5}-Dy1-O1	180.0		

Table S4: Selected bond lengths (Å) and bond angles (°) in **2**

Yb1- O1^{1}	2.2016(8)	O1^{1}-Yb1-O1^{2}	92.15(7)	O1^{3}-Yb1-O1^{5}	92.15(7)
Yb1- O1^{2}	2.2016(8)	O1-Yb1-O1^{3}	87.85(7)	O1^{2}-Yb1-O1^{4}	87.85(7)
Yb1- O1^{3}	2.2016(8)	O1^{1}-Yb1-O1^{3}	87.85(7)	O1^{2}-Yb1-O1^{5}	87.85(7)
Yb1- O1	2.2016(8)	O1^{4}-Yb1-O1^{3}	92.15(7)	O1^{2}-Yb1-O1^{3}	180.0
Yb1- O1^{4}	2.2016(8)	O1^{4}-Yb1-O1	180.0	O1^{2}-Yb1-O1	92.15(7)
Yb1- O1^{5}	2.2016(8)	O1-Yb1-O1^{5}	87.85(7)		
P1- O1	1.477(2)	O1^{1}-Yb1-O1	92.15(7)		
P1- O2	1.542(2)	O1^{1}-Yb1-O1^{4}	87.85(7)		
P1- O3	1.502(3)	O1^{4}-Yb1-O1^{5}	92.15(7)		
P1- O4	1.581(2)	O1^{1}-Yb1-O1^{5}	180.0		

Table S5: Selected bond lengths (Å) and bond angles (°) in **3**

Y1- O1^{1}	2.2259(1)	O1^{1}-Y1-O1^{2}	180.0	O1^{4}-Y1-O1^{3}	180.0
Y1- O1^{2}	2.2259(1)	O1^{1}-Y1-O1^{3}	92.39(4)	O1^{2}-Y1-O1	87.61(4)
Y1- O1^{3}	2.2259(1)	O1^{1}-Y1-O1^{4}	87.60(4)	O1^{5}-Y1-O1^{4}	92.39(4)
Y1- O1^{4}	2.2259(1)	O1-Y1-O1^{4}	87.60(4)	O1^{2}-Y1-O1^{4}	92.40(4)
Y1- O1^{5}	2.2259(1)	O1-Y1-O1^{5}	180.0	O1^{2}-Y1-O1^{5}	92.40(4)
Y1- O1	2.2259(1)	O1^{5}-Y1-O1^{3}	87.61(4)		
P1- O1	1.4894(3)	O1^{1}-Y1-O1^{5}	87.60(4)		
P1- O2	1.5564(4)	O1^{1}-Y1-O1	92.39(4)		
P1- O3	1.5081(4)	O1-Y1-O1^{3}	92.39(4)		
P1- O4	1.5871(3)	O1^{2}-Y1-O1^{3}	87.61(4)		

Table S6. Continuous Shape measures of the coordination polyhedra of Ln(III) ion of type LnL_6 for **1-3**

Complex	***HP-6***	***PPY-6***	***OC-6***	***TPR-6***	***JPPY-6***
1	30.142	28.928	**0.118**	16.507	32.286
2	30.564	29.121	**0.088**	16.527	32.512
3	30.370	29.032	**0.101**	16.517	32.408

Label	***Symmetry***	***Shape***
HP-6	D6h	Hexagon
PPY-6	C5v	Pentagonal pyramid
OC-6	Oh	Octahedron
TPR-6	D3h	Trigonal prism
JPPY-6	C5v	Johnson pentagonal pyramid J2

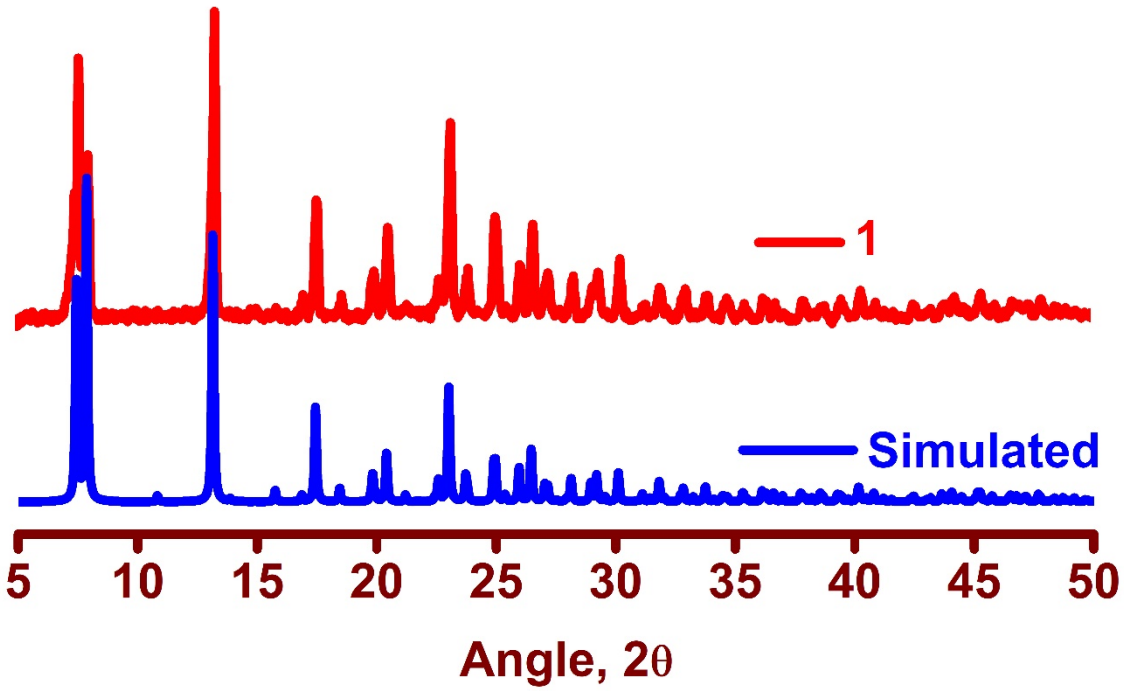

Figure S13. Simulated and experimental PXRD pattern of **1**

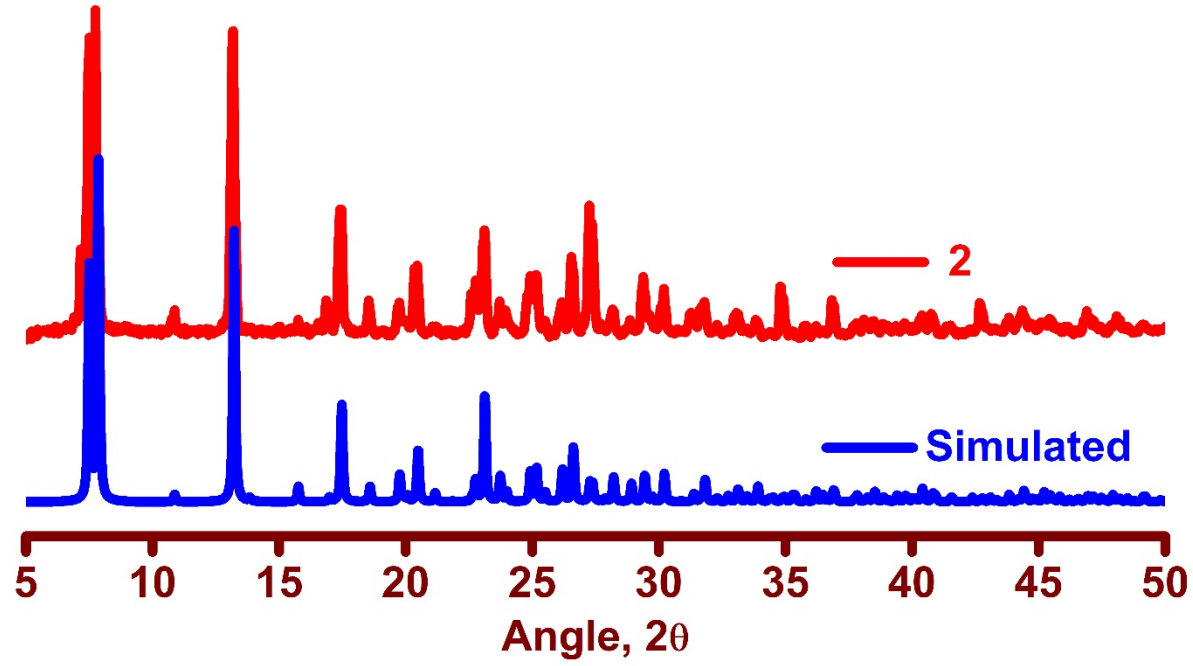

Figure S14. Simulated and experimental PXRD pattern of **2**

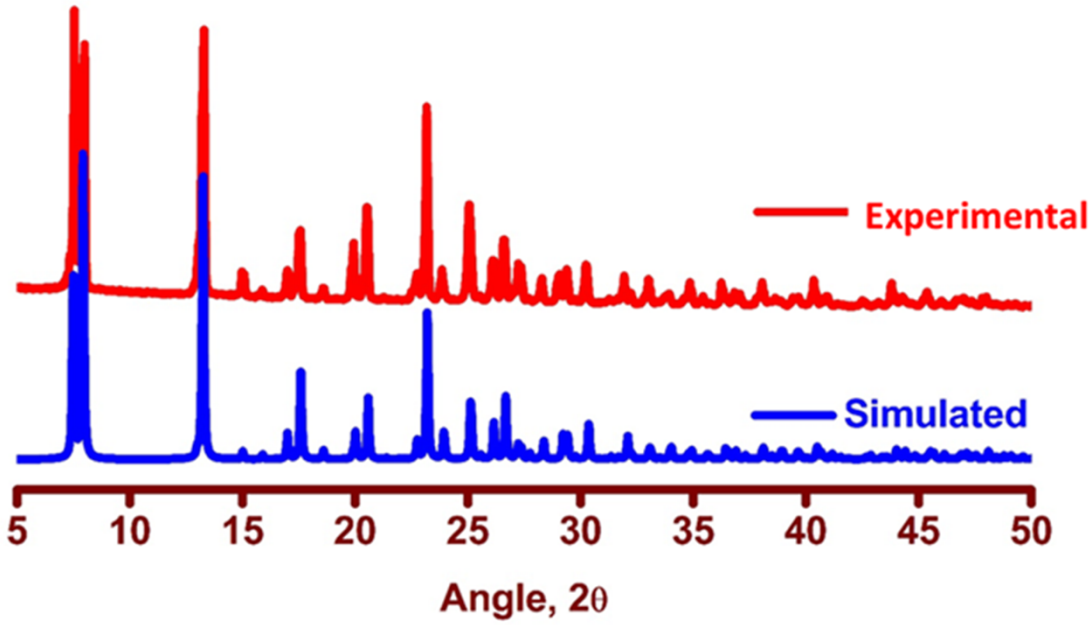

Figure S15A. Simulated and experimental PXRD pattern of **3**

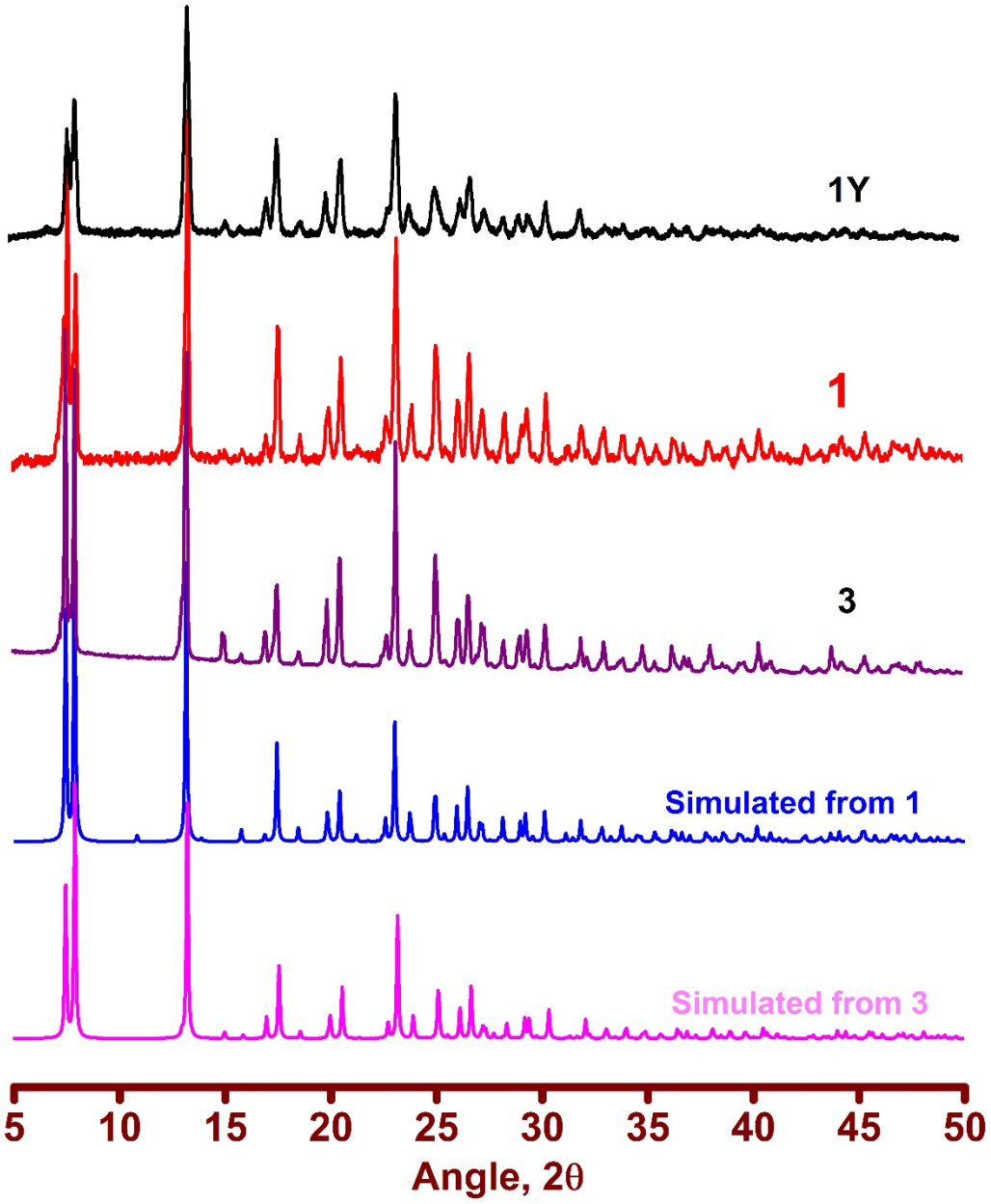

Figure S15B. Simulated and experimental PXRD pattern of **1Y**

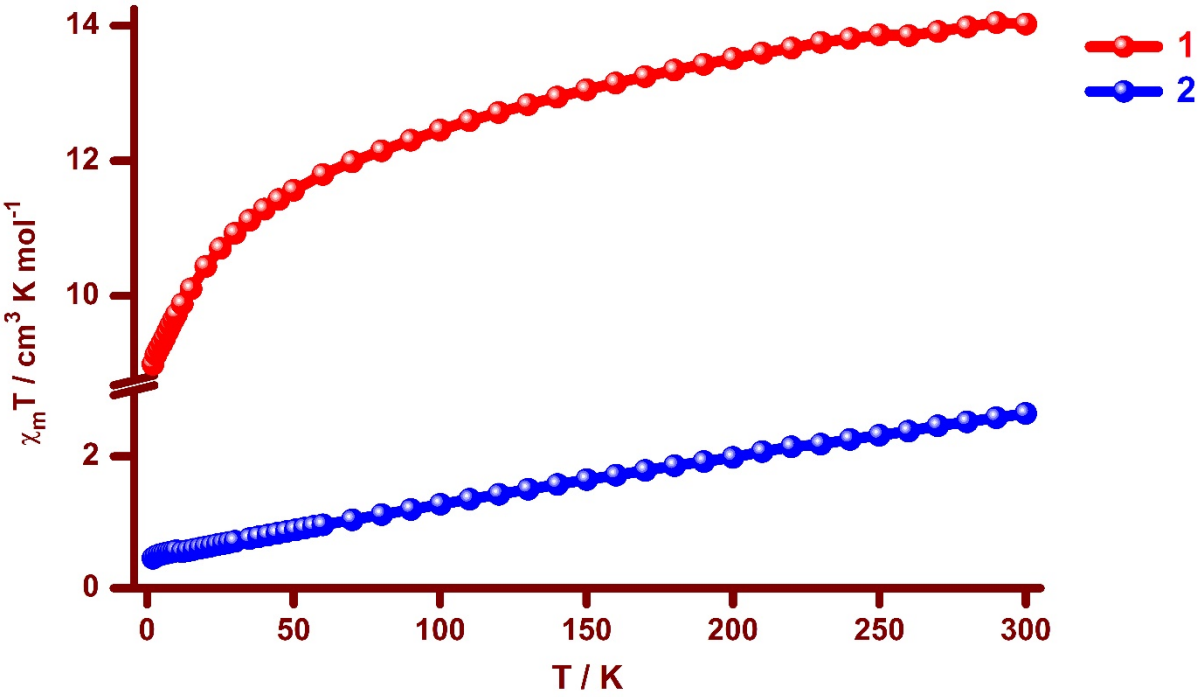

Figure S16. The temperature-dependence of $\chi_m T$ product for **1** and **2** for a temperature range of 2 – 300 K at 0.1T

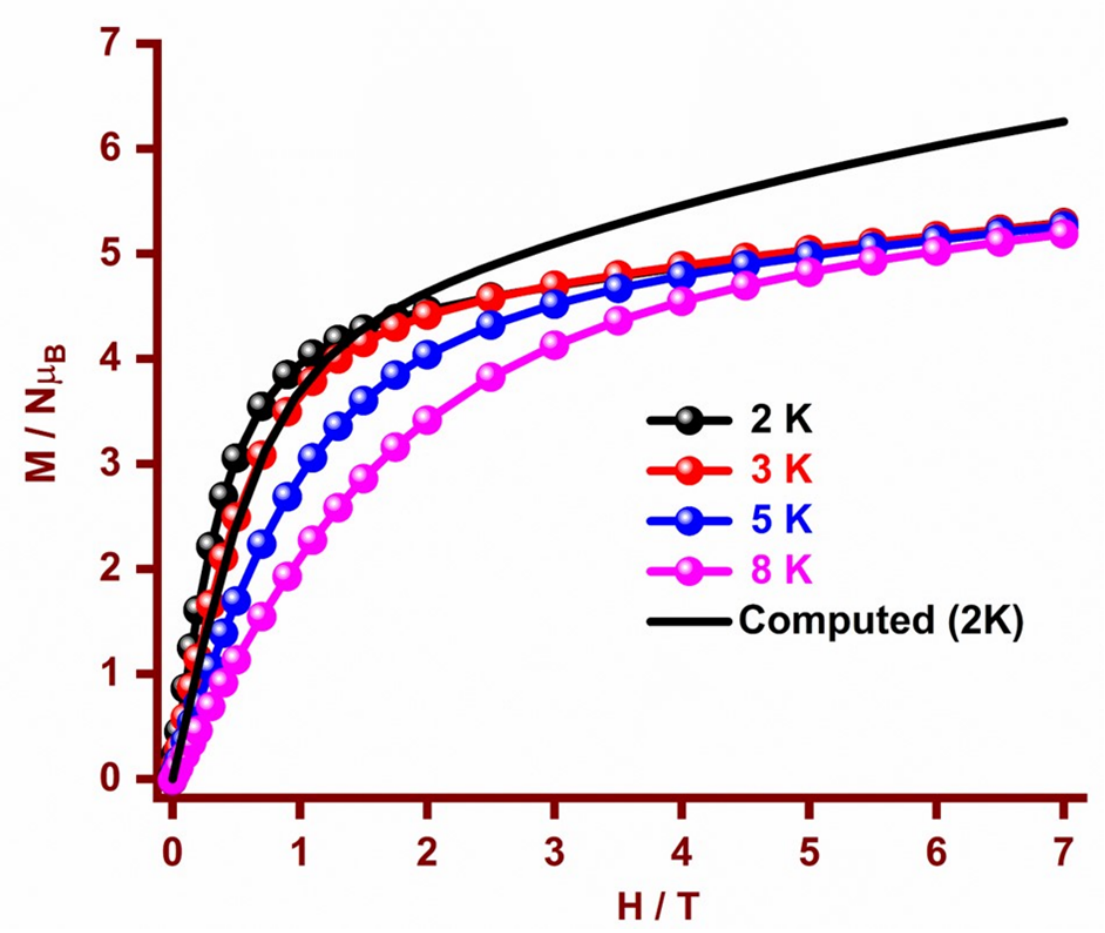

Figure S17. The field-dependence of magnetization data for **1** at 2 K, 4 K, 6 K and 8 K.

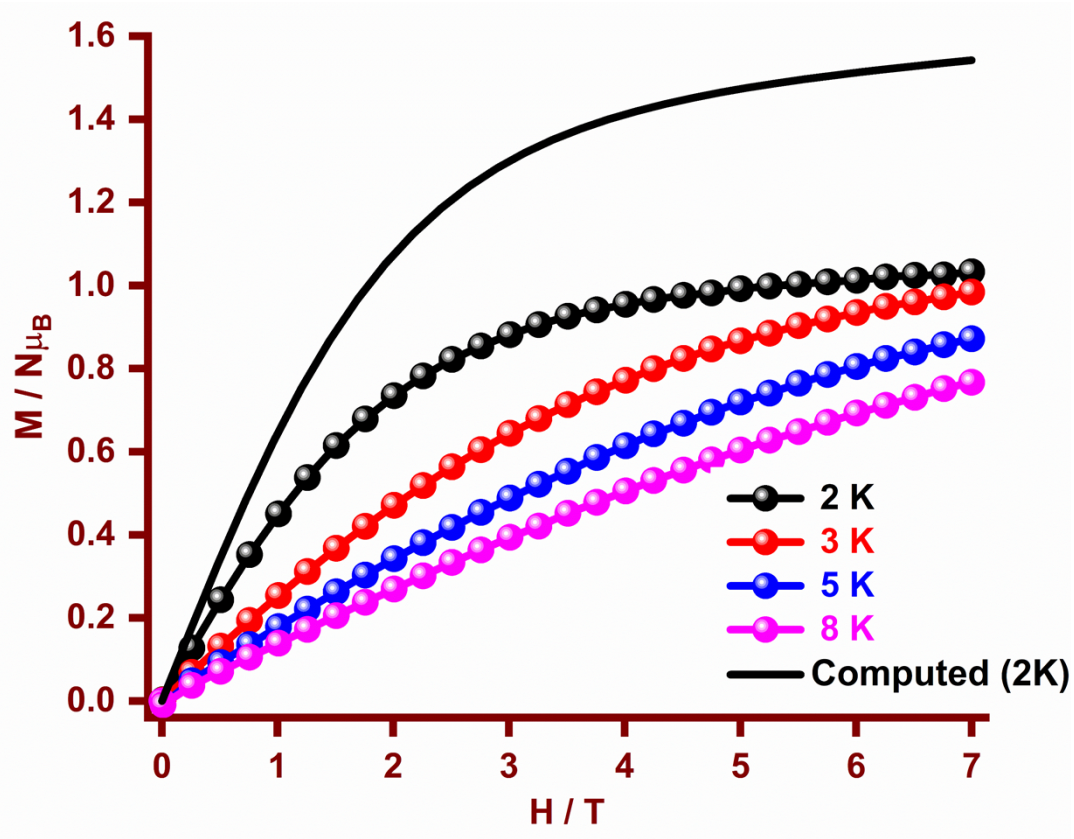

Figure S18. The field-dependence of magnetization data for **2** at 2 K, 4 K, 6 K and 8 K.

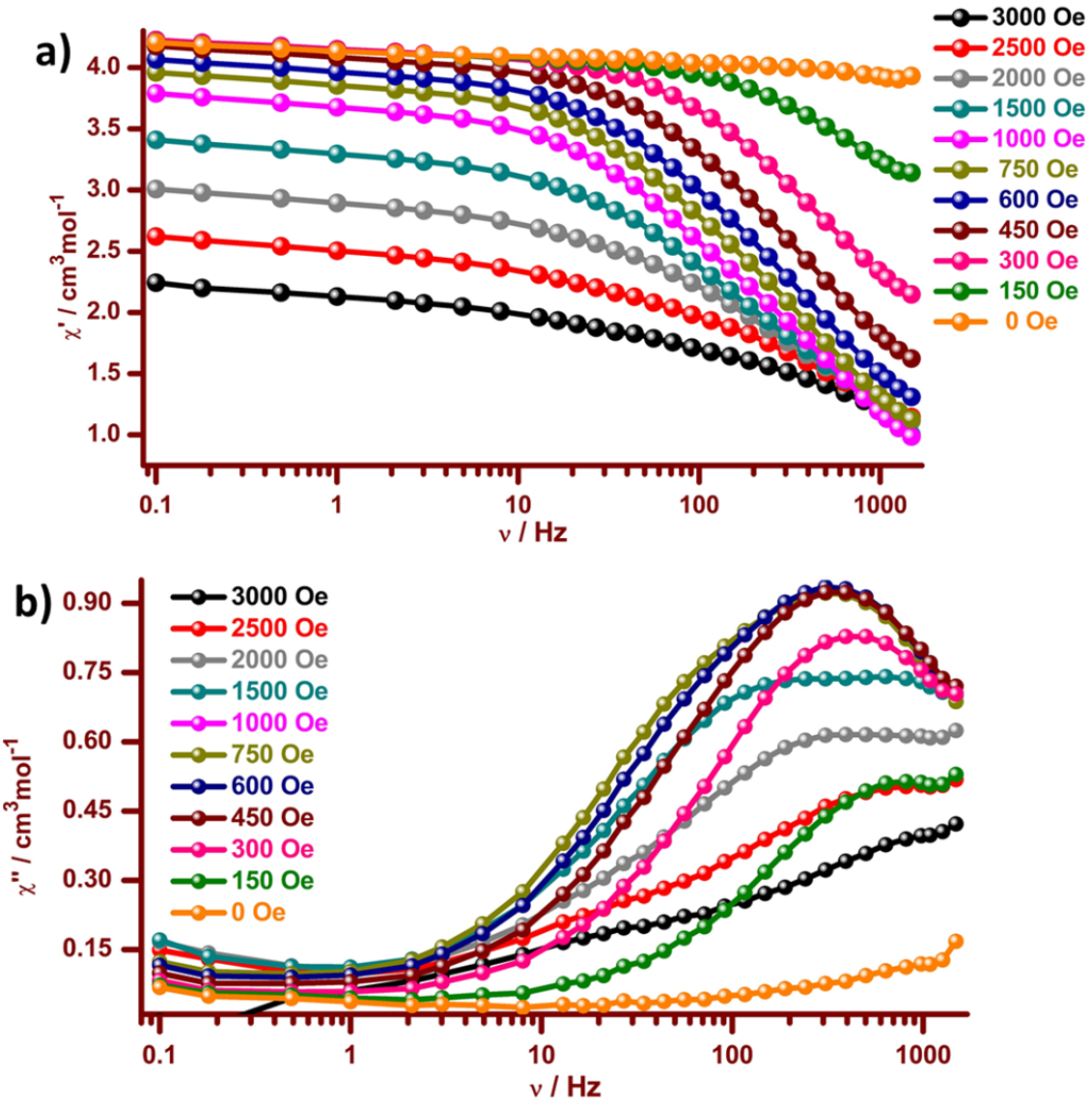

Figure S19: Frequency dependence of (a) in-phase (χ') and (b) out-of-phase (χ'') molar magnetic susceptibility for complex **1** in the presence of various dc fields at 1.8 K.

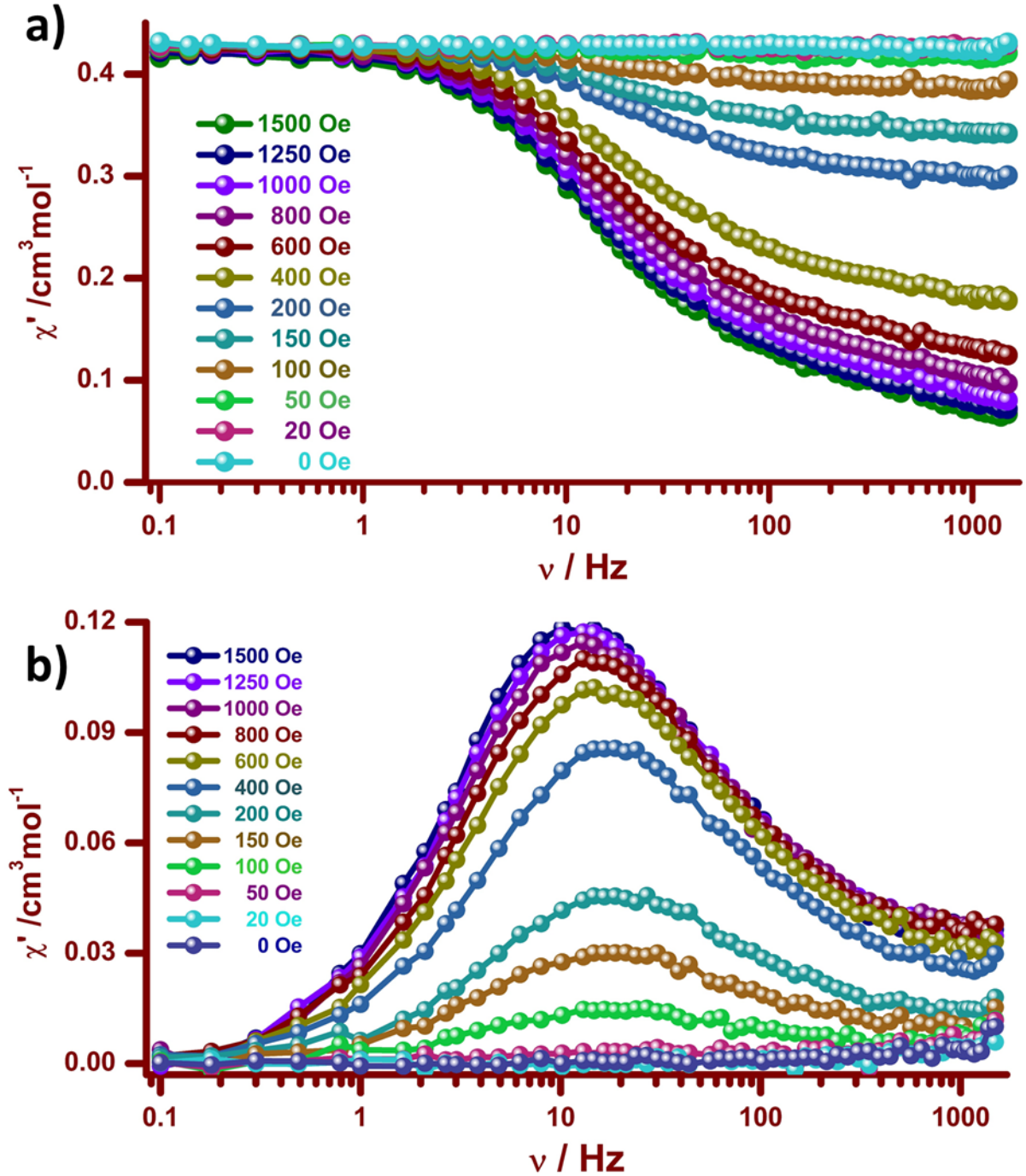

Figure S20: Frequency dependence of (a) in-phase (χ') and (b) out-of-phase (χ'') molar magnetic susceptibility for complex **2** in the presence of various dc fields at 1.8 K.

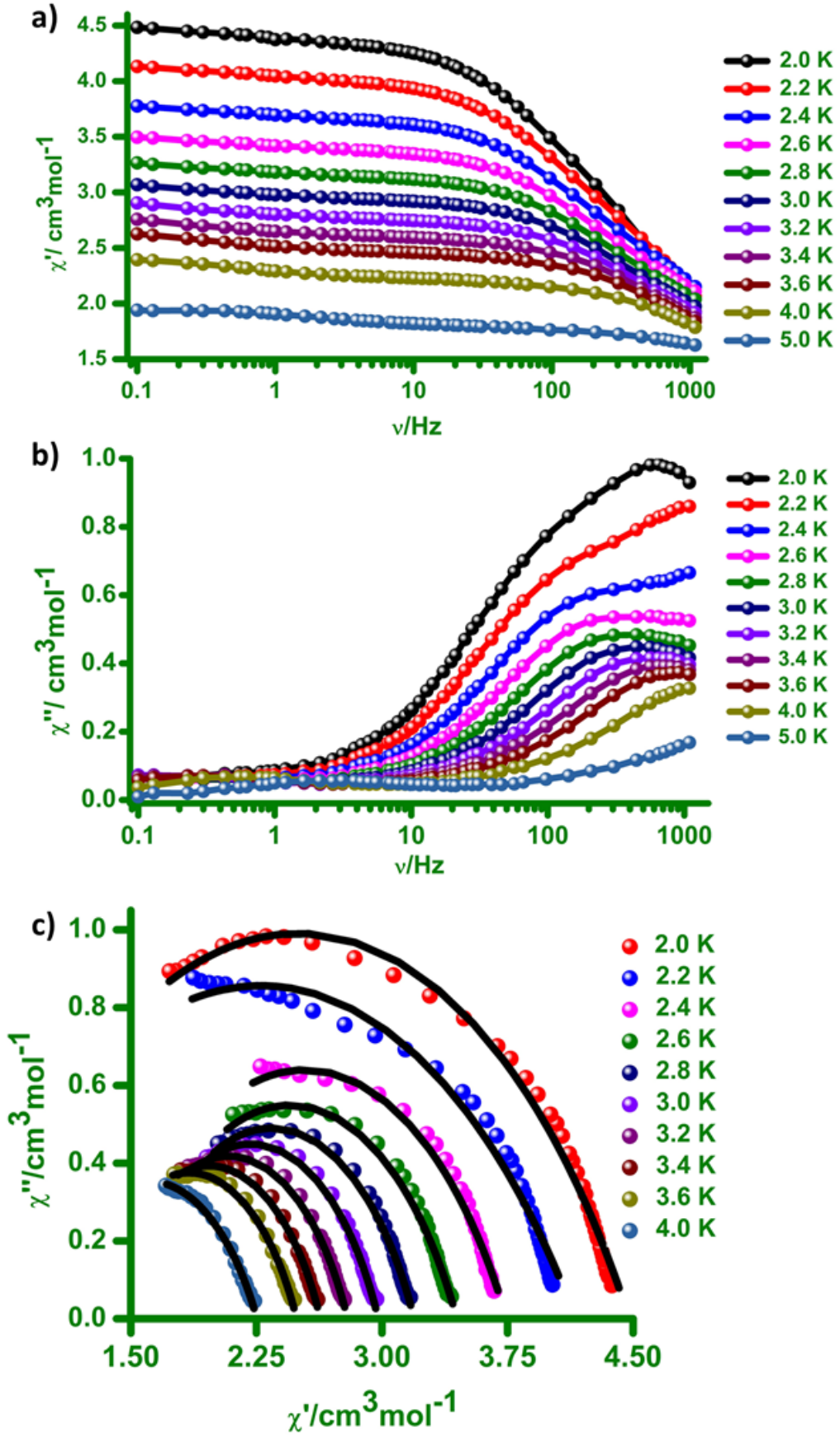

Figure S21: Frequency dependence of (a) in-phase (χ′) and (b) out-of-phase (χ′′) component of ac susceptibility (χ′) for complex **1** under an applied dc field of 600 Oe. Solid lines are guides for the eyes. (c) Cole–Cole plot for **1** under an applied dc field of 600 Oe. Solid black lines are the best fit to the Debye model.

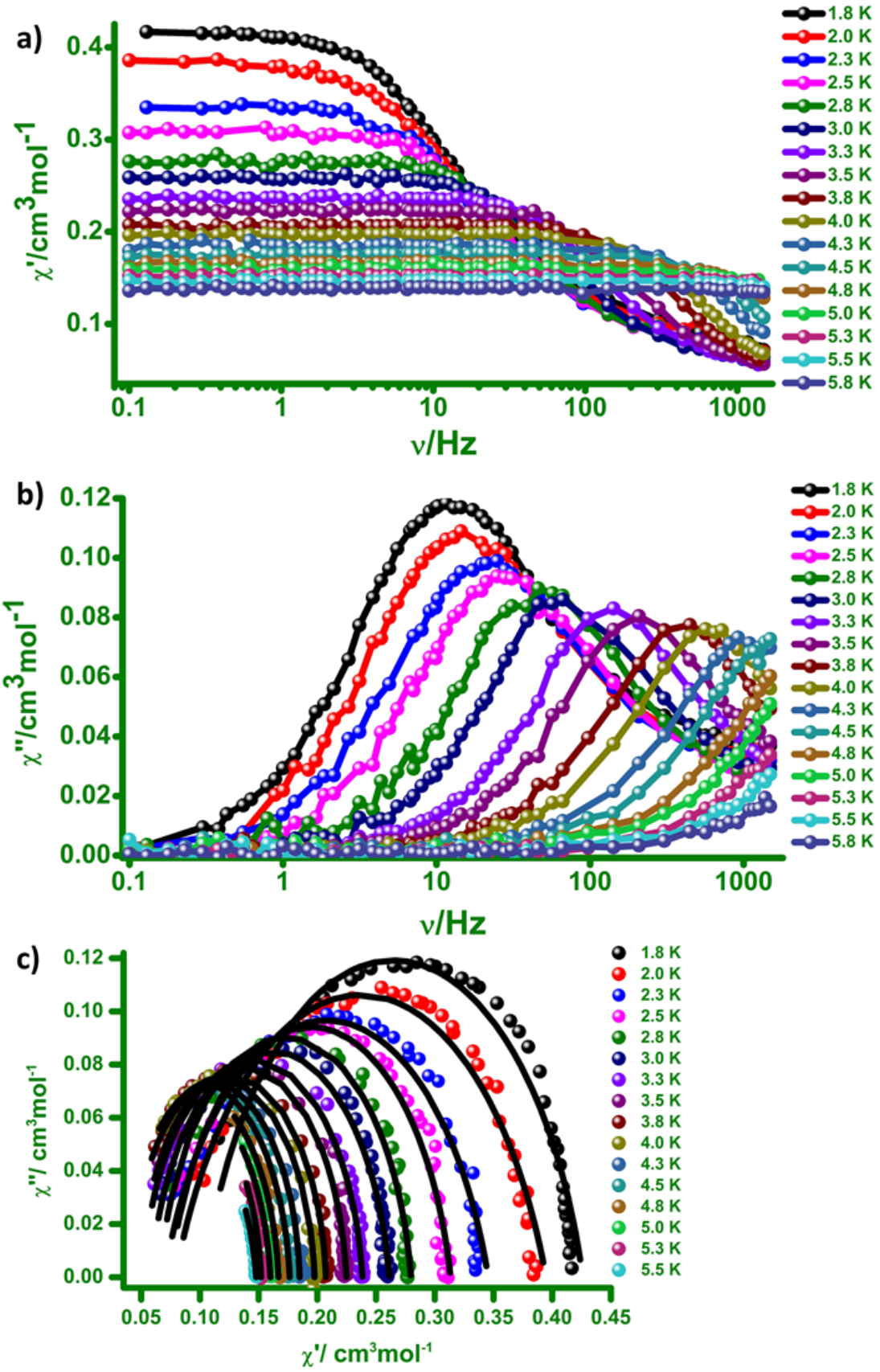

Figure S22: Frequency dependence of (a) in-phase (χ') and (b) out-of-phase (χ'') component of ac susceptibility (χ') for complex **2** under an applied dc field of 1250 Oe. Solid lines are guides for the eyes. (c) Cole–Cole plot for **2** under an applied dc field of 1250 Oe. Solid black lines are the best fit to the Debye model.

The Cole-Cole data of **1** and **4** were fitted by considering single relaxation process using the generalized Debye model, as follows:

$$\chi_{AC}(\omega) = \chi_S + \frac{\chi_T - \chi_S}{1 + (i\omega\tau)^{(1-\alpha)}} \qquad \cdots\cdots\cdots\cdots \textit{ equation-1}$$

where χ_S = adiabatic susceptibility, χ_T = isothermal susceptibility, ω=angular frequency, τ = relaxation time, and α reflects the extent of distribution of the relaxation times.

Table-S7. Fitting parameters for Cole-Cole plot for complex **1**

T/K	χ_S	χ_T	τ	α	Residual
1.8 K	0.761058E+00	0.492666E+01	0.531404E-03	0.363215E+00	0.585233E-01
2	0.524866E+00	0.447717E+01	3.82532E-4	0.408206E+00	0.420409E-01
2.2	0.398572E+00	0.415648E+01	3.83353E-4	0.455489E+00	0.639657E-01
2.4	0.133578E+01	0.374467E+01	0.383104E-03	0.377963E+00	0.279579E-01
2.6	0.145906E+01	0.344699E+01	0.381872E-03	0.356938E+00	0.177836E-01
2.8	0.149266E+01	0.319219E+01	0.361812E-03	0.333503E+00	0.880790E-02
3	0.145990E+01	0.297747E+01	0.317122E-03	0.318875E+00	0.504593E-02
3.2	0.137785E+01	0.279382E+01	0.250748E-03	0.320917E+00	0.449141E-02
3.4	0.130714E+01	0.263175E+01	0.201090E-03	0.317878E+00	0.329172E-02
3.6	0.120356E+01	0.248976E+01	0.148617E-03	0.327321E+00	0.356640E-02
4	0.956534E+00	0.225332E+01	0.708327E-04	0.364214E+00	0.375780E-02

Table-S8. Fitting parameters for Cole-Cole plot for complex **2**

T/K	χ_S	χ_T	τ	α	Residual
1.8	0.103218E+00	0.425967E+00	0.108278E-01	0.190014E+00	0.186226E-02
2	0.791662E-01	0.394756E+00	0.844039E-02	0.245822E+00	0.389625E-02
2.3	0.697924E-01	0.345546E+00	0.616722E-02	0.221907E+00	0.256096E-02
2.5	0.746769E-01	0.313461E+00	0.498719E-02	0.149690E+00	0.152594E-02
2.8	0.660137E-01	0.279710E+00	0.295711E-02	0.107070E+00	0.100764E-02
3.0	0.582417E-01	0.261336E+00	0.193360E-02	0.111153E+00	0.113370E-02
3.3	0.514301E-01	0.238390E+00	0.104315E-02	0.858915E-01	0.734463E-03
3.5	0.485349E-01	0.224722E+00	0.697391E-03	0.695691E-01	0.523376E-03
3.8	0.410826E-01	0.207304E+00	0.369060E-03	0.562898E-01	0.429946E-03
4.0	0.363905E-01	0.197599E+00	0.254023E-03	0.511523E-01	0.230986E-03
4.3	0.300863E-01	0.184863E+00	0.146137E-03	0.340834E-01	0.226204E-03
4.5	0.122971E-01	0.176467E+00	0.865507E-04	0.628120E-01	0.477218E-03
4.8	0.767135E-02	0.166871E+00	0.536928E-04	0.598151E-01	0.653958E-04
5	0.754562E-13	0.160101E+00	0.372894E-04	0.736167E-01	0.288916E-03
5.3	0.494966E-02	0.151956E+00	0.266502E-04	0.531600E-01	0.491082E-04
5.5	0.186257E-13	0.147906E+00	0.180457E-04	0.101787E+00	0.598846E-04

Computational Details:

All the ab initio calculation has been performed with MOLCAS8.2 programme package[6]. The basis set of all elements in our calculation has been taken from ANO-RCC library implemented in the above package. We have used basis set of VTZP quality for Dy and Yb, VTZ quality for metal coordinated oxygen atoms, VDZP quality for other oxygen atoms and hydrogens attached with the metal coordinated oxygen center, VDZ quality for carbon and other hydrogens. To reduce the disk space of our calculation we have used Cholesky decomposition technique. The DKH Hamiltonian was used to incorporate the spin orbit coupling of the metal center. The spin free wave functions were generated with complete active space self-consistent field (CASSCF) method. We have used CAS(9,7) and CAS (13,7) active space for Dy(III) and Yb(III) respectively which consists of nine electrons in seven 4f orbitals of Dy(III) and thirteen electrons in seven 4f orbitals of Yb(III). We have considered 21 sextets (quartets and doublets are previously found to be very high in energy and therefore the contribution to magnetic anisotropy is negligible from these states; similarly, improving the basis set was also found to have marginal improvement in the computed magnetic anisotropy parameters[7-10] and seven doublets for Dy(III) and Yb(III) in the CASSCF calculation. The spin free states were mixed by RASSI-SO to generate spin-orbit states. Finally, the energy, g tensor, magnetic properties has been calculated with SINGLE_ANISO which interfaces with RASSI-SO. The beta electron density has been plotted as a difference between the total electron density and electron density of the seven alpha electrons from the spin free states[11].

All the DFT calculation has been carried out with Gaussian09 programme package[12]. The hydrogen position optimization of the complex has been performed with replacing the anisotropic metal center by Gd(III). We have used UB3LYP functional with 6-31G** basis set for O, 6-31G* basis set C, H and CSDZ ECP[13] with its corresponding basis set for Gd in our calculation. The dispersion correction has been included in our calculation to take into account the hydrogen bonding interaction. The quadratic convergence method was followed in our calculation to get the lower energy structure.

Table S9: The computed energy and g tensor of ground eight KDs of **1**.

Energy (cm^{-1})	g_x	g_y	g_z
0.0	9.709	8.971	0.330
34.6	0.136	0.325	7.859
76.7	5.103	5.063	3.289
221.8	6.044	6.074	7.940
405.6	0.238	0.258	8.658
478.1	0.999	1.531	9.687
527.8	1.604	1.610	12.090
821.3	0.001	0.003	19.133

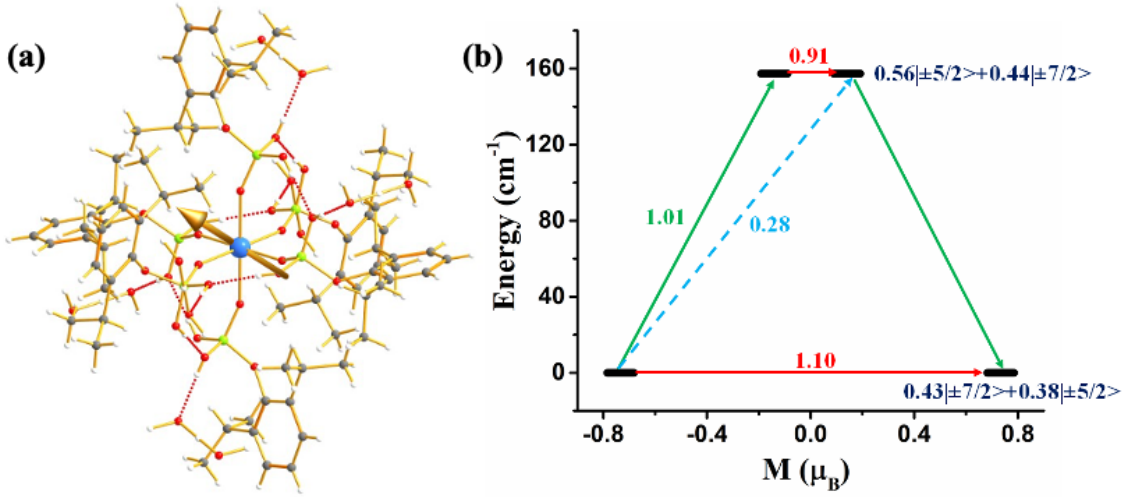

Figure S23: (a) The magnetic anisotropy axis of complex **2**. (b) The mechanism of magnetization relaxation of complex 1. The red arrow indicates QTM via the ground state and TA-QTM via the first excited state. The dotted

arrow represents the Orbach process, and the green arrow represents the possible mechanism of magnetisation relaxation. The blue characters indicate m_J composition of KDs.

Table S10: The computed energy and g tensor of ground eight KDs of **2**.

Energy (cm^{-1})	g_x	g_y	g_z
0.0	3.318	3.294	1.467
157.4	3.023	2.837	0.245
359.8	0.070	0.102	3.390
540.7	4.217	4.189	1.719

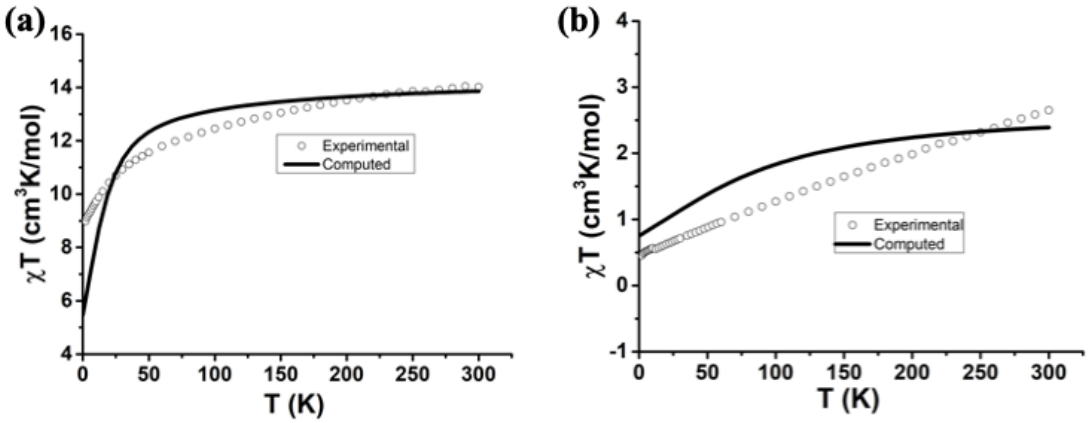

Figure S24: A comparison of experimental and computed temperature-dependent magnetic susceptibility of (a) **1** and (b) **2**.

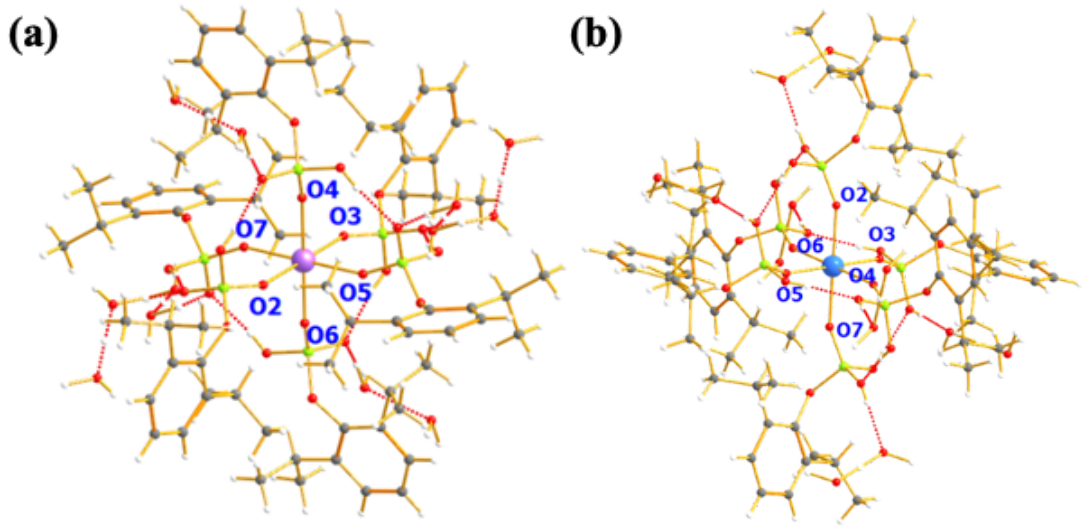

Figure S25: The LoProp charge model of complex (a) **1** and (b) **2**.

Table S11: The computed crystal field parameters of **1** and **2**.

k	q	B_k^q	
		1	**2**
2	-2	-9.66E-04	-3.17E-02
	-1	-1.07E-01	-2.57E-02
	0	2.56E+00	-8.57E+00
	1	4.21E-02	-9.87E-01
	2	-2.28E-03	-5.63E-02
4	-4	6.70E-04	3.70E-02
	-3	2.97E-01	3.75E+00
	-2	-1.99E-04	-4.33E-02
	-1	-1.21E-03	2.61E-03
	0	8.36E-03	1.26E-01
	1	4.81E-04	5.03E-02
	2	6.42E-04	-4.26E-02
	3	-1.26E-01	2.88E+00
	4	6.29E-04	2.71E-02
6	-6	-2.85E-04	3.22E-02
	-5	1.59E-05	-3.32E-03
	-4	1.05E-05	1.97E-03
	-3	6.75E-05	4.84E-03
	-2	-3.75E-06	-5.24E-04
	-1	-1.48E-05	1.00E-04
	0	5.94E-05	3.59E-03
	1	6.73E-06	3.01E-03
	2	-1.07E-05	-9.45E-04
	3	-6.79E-05	9.31E-03
	4	1.16E-05	1.58E-03
	5	-7.51E-06	1.02E-03
	6	-2.64E-04	-7.14E-03

Table S12: The LoProp charge of metal, metal-coordinated oxygens of **1** and **2**.

1		**2**	
Atom number	LoProp charge	Atom number	LoProp charge
Dy	2.6073	Yb	2.6031
O2	-1.1363	O2	-1.1131
O3	-1.1363	O3	-1.1132
O4	-1.1362	O4	-1.1132
O5	-1.1362	O5	-1.1131
O6	-1.1363	O6	-1.1132
O7	-0.7576	O7	-0.6309

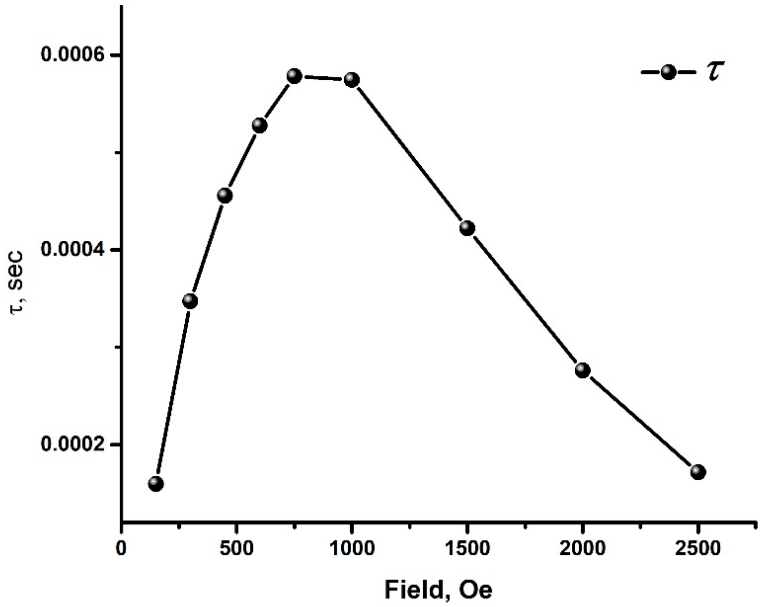

Figure 26. The variation of τ with the external magnetic field at 1.8 K for complex **1**.

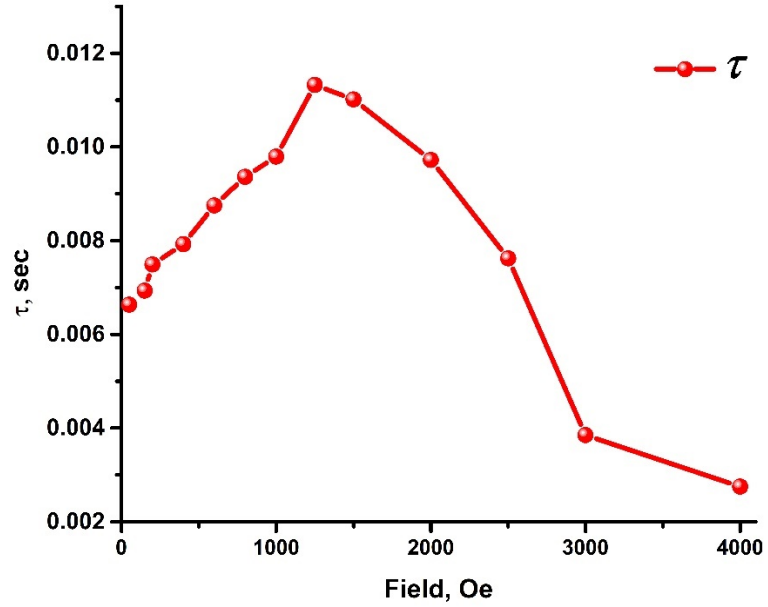

Figure 27. The variation of τ with the external magnetic field at 1.8 K for complex **2**.

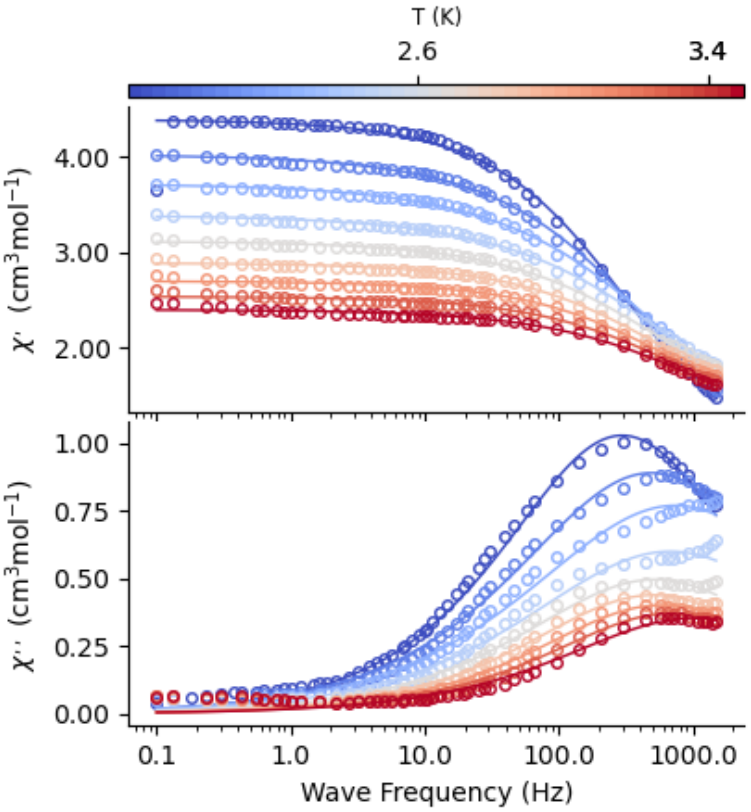

Figure S28. Frequency-dependent in-phase (top) and out-of-phase ac susceptibility (bottom) signals for **1**, solid lines represent fitted data to the experimental data (circle) with Generalized Debye equation using CC FIT2 software[14].

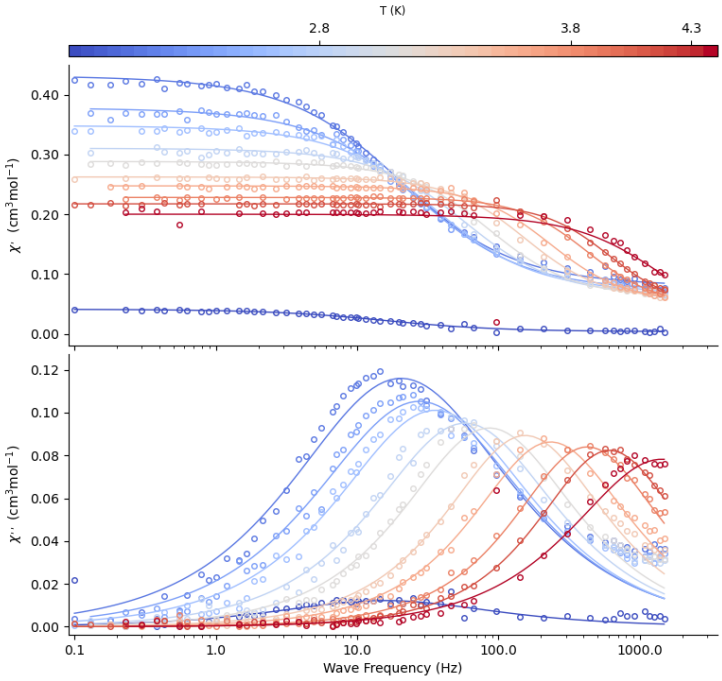

Figure S29. Frequency-dependent in-phase (top) and out-of-phase ac susceptibility (bottom) signals for **2**, solid lines represent fitted data to the experimental data (circle) with Generalized Debye equation using CC FIT2 software[14].

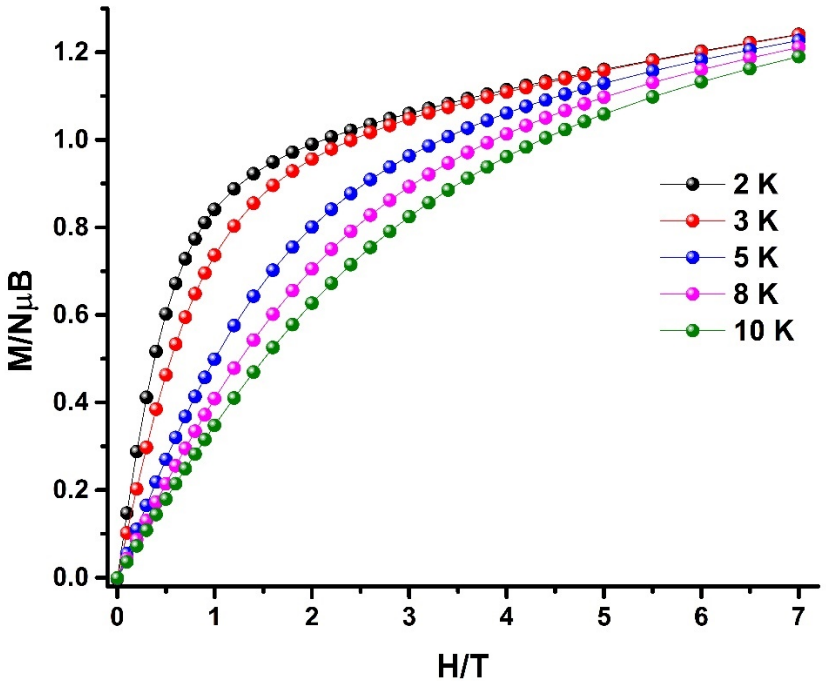

Figure S30. The field-dependence of magnetization data for **1Y** at 2 K, 4 K, 6 K, 8 K and 10 K.

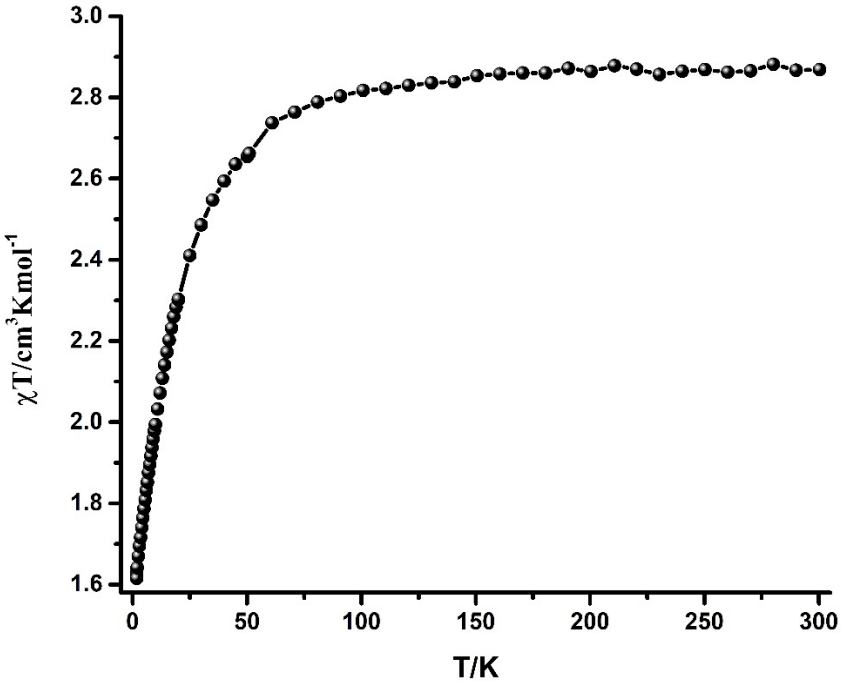

Figure S31. The temperature-dependence of $\chi_m T$ product for **1Y** for a temperature range of 2 – 300 K at 0.1T

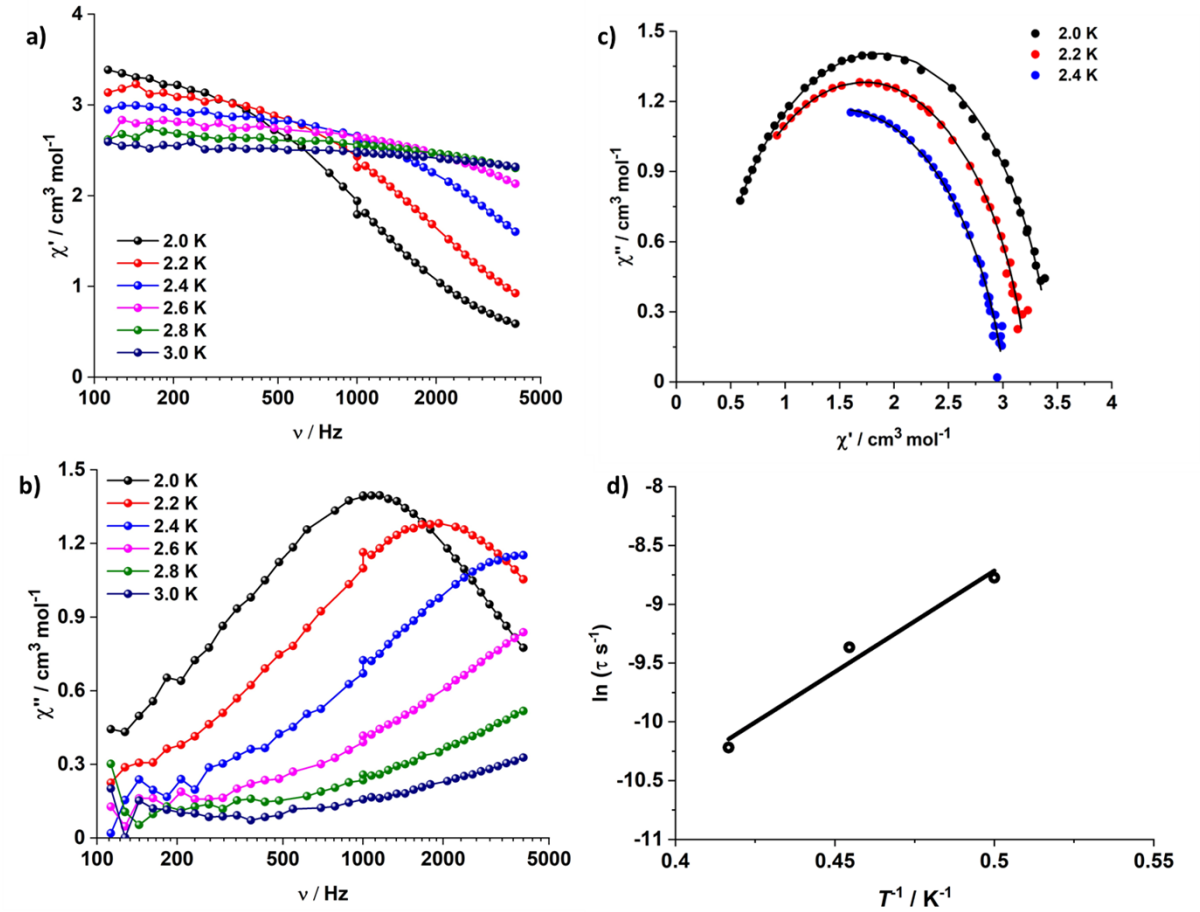

Fig S32. (a) In-phase and (b) out-of-phase ac susceptibility signals at 1500 Oe external magnetic field for (**1Y**. (c) The respective Cole-Cole plot is fitted considering a single relaxation pathway, (d) the variation of ln τ vs 1/T plot is fitted using the Arrhenius equation.

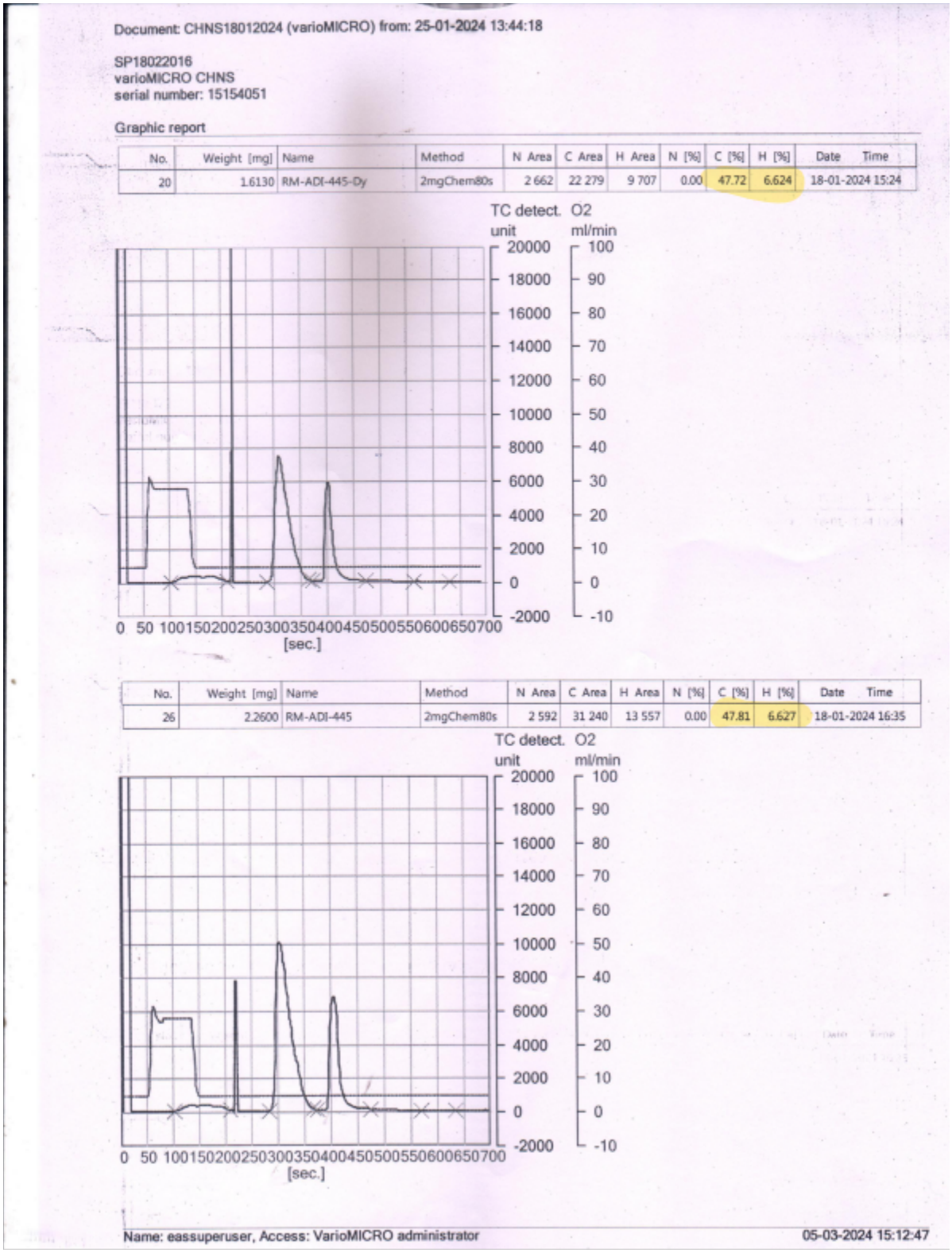

Figure S33. Elemental analysis (CHN) values for compound **1.**

References:

1. W. L. F. Armarego, *Purification of laboratory chemicals*, Butterworth-Heinemann, 2017.
2. G. M. Kosolapoff, C. K. Arpke, R. W. Lamb and H. Reich, *J. Chem. Soc. C: Organic*, 1968, 815-818.
3. O. V. Dolomanov, L. J. Bourhis, R. J. Gildea, J. A. Howard and H. Puschmann, *J. Appl. Cryst.*, 2009, **42**, 339-341.
4. G. M. Sheldrick, *Acta Crystallogr., Sect. A: Found. Adv*, 2014, **70**, C1437.
5. G. M. Sheldrick, *Acta Crystallogr. C*, 2015, **71**, 3-8.
6. F. Aquilante, J. Autschbach, R. K. Carlson, L. F. Chibotaru, M. G. Delcey, L. De Vico, I. Fdez. Galván, N. Ferré, L. M. Frutos, L. Gagliardi, M. Garavelli, A. Giussani, C. E. Hoyer, G. Li Manni, H. Lischka, D. Ma, P. Å. Malmqvist, T. Müller, A. Nenov, M. Olivucci, T. B. Pedersen, D. Peng, F. Plasser, B. Pritchard, M. Reiher, I. Rivalta, I. Schapiro, J. Segarra-Martí, M. Stenrup, D. G. Truhlar, L. Ungur, A. Valentini, S. Vancoillie, V. Veryazov, V. P. Vysotskiy, O. Weingart, F. Zapata and R. Lindh, *J. Comput. Chem.*, 2016, **37**, 506-541.
7. K. Bernot, J. Luzon, L. Bogani, M. Etienne, C. Sangregorio, M. Shanmugam, A. Caneschi, R. Sessoli and D. Gatteschi, *J. Am. Chem. Soc.*, 2009, **131**, 5573-5579.
8. J. Liu, Y.-C. Chen, J.-L. Liu, V. Vieru, L. Ungur, J.-H. Jia, L. F. Chibotaru, Y. Lan, W. Wernsdorfer and S. Gao, *J. Am. Chem. Soc.*, 2016, **138**, 5441-5450.
9. C. A. Goodwin, F. Ortu, D. Reta, N. F. Chilton and D. P. Mills, *Nature*, 2017, **548**, 439-442.
10. T. Gupta and G. Rajaraman, *European Journal of Inorganic Chemistry*, 2018, **2018**, 3402-3412.
11. D. Aravena and E. Ruiz, *Inorg. Chem.*, 2013, **52**, 13770-13778.
12. M. Frisch, G. Trucks, H. B. Schlegel, G. E. Scuseria, M. A. Robb, J. R. Cheeseman, G. Scalmani, V. Barone, B. Mennucci and G. Petersson, *Journal*, 2009.
13. T. R. Cundari and W. J. Stevens, *J. Chem. Phys.*, 1993, **98**, 5555-5565.
14. D. Reta and N. F. Chilton, *Physical Chemistry Chemical Physics*, 2019, **21**, 23567-23575.